Materials Today Bio 25 (2024) 100988

Contents lists available at ScienceDirect

Materials Today Bio

journal homepage: www.journals.elsevier.com/materials-today-bio

Durable protective efficiency provide by mRNA vaccines require robust immune memory to antigens and weak immune memory to lipid nanoparticles

Xueying Tang, Jiashuo Zhang, Dezhi Sui, Zihan Xu, Qiongfen Yang, Tianyu Wang, Xiaoya Li, Xinrong Liu, Yihui Deng [*,1], Yanzhi Song [**,1]

College of Pharmacy, Shenyang Pharmaceutical University, Shenyang, Liaoning, 110016, China

ARTICLE INFO

Keywords:
mRNA cancer vaccine
Immune memory
Lipid nanoparticles
Sialic acid
Tumor immune cycle

ABSTRACT

The Pegylated lipids in lipid nanoparticle (LNPs) vaccines have been found to cause acute hypersensitivity reactions in recipients, and generate *anti*-LNPs immunity after repeated administration, thereby reducing vaccine effectiveness. To overcome these challenges, we developed a new type of LNPs vaccine (SAPC-LNPs) which was co-modified with sialic acid (SA) - lipid derivative and cleavable PEG - lipid derivative. This kind of mRNA vaccine can target dendritic cells (DCs) and rapidly escape from early endosomes (EE) and lysosomes with a total endosomal escape rate up to 98 %. Additionally, the PEG component in SAPC-LNPs was designed to detach from the LNPs under the catalysis of carboxylesterase in vivo, which reduced the probability of PEG being attached to LNPs entering antigen-presenting cells. Compared with commercially formulated vaccines (1.5PD-LNPs), mice treated with SAPC-LNPs generated a more robust immune memory to tumor antigens and a weaker immune memory response to LNPs, and showed lower side effects and long-lasting protective efficiency. We also discovered that the anti-tumor immune memory formed by SAPC-LNPs mRNA vaccine was directly involved in the immune cycle to rattack tumor. This immune memory continued to strengthen with multiple cycles, supporting that the immune memory should be incorporated into the theory of tumor immune cycle.

1. Introduction

The mRNA therapy is revolutionizing the field of medicine. mRNA1273 and BNT162 have played vital roles in combating the rapid spread of COVID-19. In addition to their success in COVID-19 treatment, recent reports have shown that mRNA-4157 (NCT05933577) and BNT1221 are achieving remarkable clinical results in cancer therapy. Lipid nanoparticles (LNPs) have proved to be powerful tools for RNA delivery, including mRNA [1–3]. However, the wide use of uncleavable PEG lipids (such as 1,2-dimyristyl-RAC-glycerol-3-methoxy polyethylene glycol, $mPEG_{2000}DMG$) has been proved to cause a series of questions, including attenuate cellular uptake, hinder lysosomal escape [4] and produce accelerated blood clearance (ABC) phenomenon [5], which has negative impacts on RNA delivery platforms based on LNPs [6]. Recent data showed that anti-PEG IgG and IgM significantly boosted 13.1-fold and 68.5-fold, respectively, following mRNA-1273 vaccination [7], and may cause more intense side effects when repeatedly injected mRNA vaccines [8]. More importantly, the mRNA vaccines for cancer therapy and prevention generally required more frequent repeated administration than COVID-19 vaccines, which will induce a higher level of anti-PEG antibody, leading to impaired protein expression and therapeutic effects of followed administration, and even induce hypersensitivity reactions (HSRs) that may endanger the life of patients [9–11]. Therefore, it is necessary to further optimize the formulation of LNPs to develop safer and more effective mRNA tumor vaccines.

Currently, the research of LNPs is focused on optimizing the structure of ionizable lipids. However, this optimization often fails to achieve simultaneous improvements in cellular uptake, endosome escape, organ

* Corresponding author.
** Corresponding author.
E-mail addresses: 2110325731@qq.com (X. Tang), 2545318567@qq.com (J. Zhang), 1874469634@qq.com (D. Sui), 863394293@qq.com (Z. Xu), 1967556433@qq.com (Q. Yang), 1157140348@qq.com (T. Wang), 1546013684@qq.com (X. Li), 13898891331@163.com (X. Liu), dengyihui@syphu.edu.cn (Y. Deng), songyanzhi@syphu.edu.cn (Y. Song).
[1] Present/permanent address: School of Pharmacy, Shenyang Pharmaceutical University, 103 Wenhua Road, Shenyang, Liaoning 110,016, China.

https://doi.org/10.1016/j.mtbio.2024.100988
Received 18 September 2023; Received in revised form 24 January 2024; Accepted 31 January 2024
Available online 9 February 2024

targeting, and cell targeting. For example, the Lipid 5 designed by Sabnis et al. [12] exhibit higher endosomal escape efficiency compared to MC3 lipid but has been found to reduce cell uptake efficiency. In addition, SORT lipids with organ-targeting ability may experience decreased endosomal escape efficiency when a large number of anionic lipids are introduced during spleen targeting [13,14]. More importantly, it is important to consider that immune memory plays a crucial role in the protective immunity provided by vaccines [15]. Nevertheless, current studies have overlooked the immunogenicity of LNPs and their potential for being recognized by the immune system. LNPs are primarily distributed in the liver [16–18], and incorporating uncleavable $mPEG_{2000}DMG$ into LNPs may enhance Kupffer cells' immune memory towards LNPs in the liver while accelerating phagocytosis and elimination of PEGylation LNPs by Kupffer cells upon secondary administration [19]. Therefore, finding ways to enhance antigen-specific immune memory while reducing memory towards LNPs is essential for mRNA cancer vaccines to provide long-lasting protection; however, researchers have not yet addressed this point.

In this study, we replaced uncleavable PEG-lipid ($mPEG_{2000}DMG$) with cleavable PEG-lipid ($mPEG_{2000}CHS$, PC) LNPs and co-modified them with sialic acid (SA) lipid derivatives to target dendritic cells (DCs). We found that lipid nanoparticles co-modified with SA and cleavable PEG lipids (SAPC-LNPs) can effectively target DCs and improve transfection efficiency in DCs. It was also unexpectedly found that SA promoted the endosome escape of SAPC-LNPs, with a total endosomal escape efficiency of up to 98 %, significantly better than 1.5PD-LNPs (only 70 %) formulated in commercially available formulations. The mice vaccinated with the SAPC-LNPs vaccine achieved nearly 90 % protection against multiple tumor cell attacks over a year, which was significantly higher than that of the commercially formulated mRNA vaccine (62.5 %). The SAPC-LNPs promote maturation and migration of DCs, enhance antigen presentation to naïve T cells, and generate more central memory T cells (T_{CM}). The immunogenicity of LNPs itself is weakened by using the cleavable PEG-lipid, resulting in a weak immune memory response to LNPs but a robust immune memory response to antigens. This ensures that the production of mRNA-encoded proteins is not significantly reduced and alleviates side effects after repeated injection of SAPC-LNPs. We found that the phenotype of memory T cells formed after vaccination may be related to the long-lasting protective efficacy of the SAPC-LNPs mRNA vaccine. An increase in the proportion of TCM could serve as an indicator for assessing the long-lasting efficacy of vaccine. The ratio of TCM to effector memory T cells (TEM) can be used to assess the long-lasting efficacy of vaccines. More importantly, we have improved upon the theory of tumor immune cycle by incorporating immune memory as a new event into the tumor immune cycle, dividing the tumor immune cycle into a large cycle and a small cycle. We hypothesize that as the tumor immune cycle progresses positively, enhanced immune memory will accompany tumor regression.

2. Materials and method

2.1. Materials

The ionizable lipid DLin-MC3-DMA, 1,2-dioctadecanoyl-*sn*-glycero-3-phosphocholine (DSPC), cholesterol (CH), 1,2-dimrystoyl-*rac*-glycero, and methoxyethylene glycol 2000 ether ($mPEG_{2000}$-DMG) were purchased from AVT Pharmaceutical Technology Co., LTD (Shanghai, China). Ovalbumin (OVA) mRNA was obtained from TriLink Biotechnology, Inc. All the mRNA were modified with 5-methylcytidine. Enhanced green fluorescent protein (EGFP) and firefly luciferase (Luc) mRNA were purchased from APExBIO Technology LLC (Houston, Texas, USA). SA-CH and $mPEG_{2000}$-CHS were synthesized in our laboratory (Supplementary Information).

2.2. Method

2.2.1. Preparation and characterization of mRNA LNPs

The mRNA-loaded LNPs were prepared by microfluidic mixing [20,21]. The lipid mixture (13.5 mM) was dissolved in ethanol. The mRNA was dissolved in RNase-free citrate buffer (50 mM, pH = 4.0). The aqueous mRNA solution was rapidly mixed with the lipid mixture at 3:1 a volume (total flow rate 2.4 mL/min) using a microfluidic mixing device (LNP-B1, FluidicLab, Shanghai, China) with N/P = 8.0 (26.7/1, wt/wt, lipid/RNA). The lipid solution of the SAPC-LNPs contain DLin-MC3-DMA/DSPC/CH/SA-CH/$mPEG_{2000}$CHS = 40/10/39.8/10/0.2. The lipid mixtures of PC-LNPs, 1.5PD-LNPs and SAPD-LNPs were DLin-MC3-DMA/DSPC/CH/$mPEG_{2000}$CHS (40/10/49.8/0.2), DLin-MC3-DMA/DSPC/CH/$mPEG_{2000}$DMG (40/10/48.5/1.5), and DLin-MC3-DMA/DSPC/CH/-SA-CH/$mPEG_{2000}$DMG = 40/10/39.8/10/0.2, respectively. $mPEG_{2000}$ CHS was replaced with an equimolar amount of $mPEG_{2000}$DMG in the PC-LNPs formulation to obtain 0.2PD-LNPs. 1 % molar of cholesterol was replaced with equimolar DiI or DiD to obtain DiI or DiD–labeled LNPs. The initial LNPs were rapidly diluted 30-fold with RNase-free 1 × PBS and then concentrated (75 μg mRNA/mL) by Amico Ultra-15 filters (30 kDa, Millipore). For particle size (Nicomp 380) and zeta potential measurements (Malvern Zetasizer Nano ZS), the LNPs were diluted with 10-fold 1 × PBS and 20-fold ddH_2O, respectively. The LNPs were 5-fold concentrated for morphology observation by cryo-TEM (FEI Talos F200C). The encapsulation efficiency was measured by a Quanti-it™ RiboGreen RNA assay kit (Thermo Fisher Co., LTD). The RNA obtained in samples without Triton X-100 was interpreted as unencapsulated mRNA ($C_{unencapsulated}$), and the RNA in samples treated with 2 % TritonX-100 represented total RNA (C_{total}). The encapsulation Efficiency can be calculated by:

$$\text{Encapsulation Efficiency } (EE\%) = \frac{C_{total}\text{-}C_{unencapsulated}}{C_{total}} \times 100\%$$

2.2.2. In vitro EGFP mRNA transfection assay

DC2.4 cells or RAW264.7 cells (2×10^5/well) were inoculated into 6-well plates and cultured in RPMI-1640 complete medium (same as the cellular uptake assay) for 12 h. The EGFP mRNA–loaded LNPs were incubated with the cells for 4, 8, and 24 h (1 μg/mL EGFP mRNA) [22], washed with 1 × PBS for three times, fresh culture medium was added, and the cells were cultured for 20, 16, and 0 h, collected cells for flow cytometry analysis. For analysis by confocal laser microscopy (CSLM, ZEISS LSM880, Germany), DC2.4 cells were seeded on cell slides (NETs) and incubated with EGFP mRNA loaded LNPs (1 μg/mL EGFP mRNA) for 24 h, following fixed (4 % polyformaldehyde) and DAPI (50 μL) stained.

2.2.3. Early endosome and lysosomal escape assay

DC2.4 cells (4×10^4) were seeded in a culture dish, and DiD-labeled mRNA LNPs (250 ng/mL) were incubated with DC2.4 cells for 2 h. Lysosomes were stained with Lysotracker Green® (50 nM) for 60 min at 37 °C, washed with 1 × PBS for three times, followed by DAPI staining. For EE staining, DC2.4 cells (4×10^4) were fixed with 4 % formaldehyde (without methanol) for 15 min after 2 h incubation with DiD-labeled mRNA LNPs (250 ng/mL). They were then incubated overnight at dark conditions with anti-rabbit EEA1 primary antibodies (Cell Signaling, #3288S; diluted to a ratio of 1:100), washed three times using PBS, followed by a 2-h incubation in the dark at RT with goat Anti-Rabbit IgG(H + L)-Alexa Fluor488 secondary antibody(Cell Signaling, #237695; diluted to a ratio of1:500). The cells were washed three times using PBS and then subjected to DAPI staining. The images were obtained using CSLM(ZEISS LSM880, Germany) under magnification of1000-fold. The total endosome escape efficiency (teE) = eEE+ (100%-eEE) × eLyso (eLyso: escape efficiency of lysosomes; eEE: escape efficiency of early endosome).

The eEE and eLyso of LNPs was calculated by the following calculation formula :

eEE / eLyso = (Area of red fluorescence in a single cell − Area of yellow fluorescence in a single cell) / Area of red fluorescence in a single cell × 100%

2.2.4. Evaluation of DCs maturation and migration rate

DC2.4 cells (2×10^5 cells/well) were inoculated in a 6-well plate and incubated with SAPC-LNPs/OVA mRNA or PC-LNPs/OVA mRNA (1 μg/mL OVA mRNA) at 37 °C for 24 h. DC2.4 cells (2×10^5 cells/well) were inoculated in a 6-well plate, and incubated with SAPC-LNPs/OVA mRNA or PC-LNPs/OVA mRNA (1 μg/mL OVA mRNA) at 37 °C for 24 h washed for three times with 1 × PBS, stained with APC anti-mouse CD86 (eBioscience, 2,389,535) and APC anti-mouse MHC-I (eBioscience, 2378047) at 4 °C for 30 min in the dark, washed for 3 times. Cells were harvested for flow cytometric analysis. Cells incubated with an equal volume of 1 × PBS were used as controls. Changes in cell morphology were observed using an inverted microscope with a 40× objective lens. The co-localization of LNPs with EE was measured using the ImageJ (NIH, USA) software.

For the migration assay, DC2.4 cells (1×10^5), washed twice with PBS two times each, were added to the upper chamber of a Transwell (8 μm pore size, PC membrane). FBS-free medium containing CCL19 and CCL21 at a concentration of 250 ng/mL was added to the lower chamber. SAPC-LNPs/OVA mRNA and PC-LNPs/OVA mRNA were co-incubated with the cells at a concentration of 1 μg/mL each. After incubating for 24 h, the liquid in the chambers was removed and the cells were washed with PBS. Then they were fixed with PFA solution (4 %) for 20 min and stained using a crystal violet solution (0.1 %). The cells above the PC membrane were removed while those at the bottom of it were observed under a microscope (NIB-100, NOVEL, China). The total stained cells were decolorized using acetic acid solution (10 %) and their absorbance was measured at wavelength of 550 nm.

2.2.5. Hemolysis test

Red blood cells (RBC) are a model system for detecting membrane fusion due to their similar lipid bilayer structure to the endosome [23]. The blood of C57BL/6 mice (20 ± 2 g, male) was collected into the anticoagulant tube, and centrifuged at 1000 rpm for 10 min. The upper plasma was discarded, and the red blood cells were collected and washed three times with an equal volume of PBS (centrifuge at 500 g for 10 min). A 4 % RBC suspension was prepared by adding 160 μL of RBCs into 3840 μL of either a 1 × PBS or a citric acid buffer (including130 mM NaCl, pH 5.5), respectively. Then, incubate with mRNA-loaded SAPC-LNPs or PC-LNPs (100 μL each) along with the RBC suspension at 37 °C for 80 min (n = 3). After centrifugation at4°Cand1000gfor5min, transfer the supernatant to a 96-well plate with150 μL per well and detect it using a multifunctional board reader at 540 nm. Positive and negative controls were administered with 0.1 % Triton-X and 1 × PBS, respectively.

2.2.6. In vivo targeting study

For the in vivo targeting study, male C57BL/6 mice (20 ± 2 g) were subcutaneously injected with Fluc mRNA-loaded 1.5PD-LNPs, PC-LNPs, and SAPC-LNPs (10 μg/mouse, n = 3). D-fluorescein potassium (3 mg/100 μL) was injected intraperitoneally at 24 h. The popliteal lymph nodes of the mice were collected for bioluminescence imaging 10 min later using a Xenogen IVIS Spectrum Imaging System (Perkin Elmer, USA).

Another group of male C57BL/6 mice weighing 20 ± 2 g were subcutaneously injected with EGFP mRNA loaded into 1.5PD-LNPs, PC-LNPs, SAPC-LNPs, or PBS at a dose of 10 μg/mouse. The popliteal lymph nodes of the mice were collected to prepare single cell suspensions. The lymph nodes were gently ground on 70 μm cell mesh strainers and then centrifuged at 4 °C for 10 min at a speed of 500 g. The cells were precipitated and resuspended in PBS. For each test, APC anti-mouse MHC-II (eBioscience) and PE anti-mouse CD11c (eBioscience) antibodies were added according to the protocol and incubated for 30 min at 4 °C. The cell precipitate was resuspended in PBS for flow cytometry analysis. The sections were stained with primary antibodies against CD169, followed by immunostaining using PE-conjugated secondary antibodies and DAPI staining to visualize the nuclei.

2.2.7. In vivo immunoprophylactic vaccination

C57BL/6 mice (20 ± 2 g, male) were vaccinated with OVA mRNA-loaded SAPC-LNPs, PC-LNPs, 1.5PD-LNPs, Naked OVA mRNA and EGFP mRNA-loaded SAPC-LNPs at day 1 and 14 (10 μg/mouse, s.c). Mice treated with PBS were used as controls. Seven days after the final immunization, B16-OVA cells (3×10^5) were inoculated into the right flank of the mice. The tumor-inoculated sites were monitored daily and the time of first appearance was recorded. Tumor size was calculated using the formula: 1/2(length × widthˆ2). Tumor cells were rechallenged in tumor-free mice on days 7, 40, 125, and 180 after the last immunization. All animal experiments complied with the National Institutes of Health guide for the care and use of laboratory animals.

2.2.8. Serum antibody detection

C57BL/6 mice (20 ± 2 g, male) were subcutaneously immunized with two doses of OVA mRNA-loaded SAPC-LNPs, PC-LNPs, and 1.5PD-LNPs (10 μg/mouse) at an interval of 14 days. Blood was collected from the orbital vein on day 14, 47, and 132 after secondary immunization and centrifuged at 4 °C for 10 min at a speed of 3000 rpm to obtain serum. OVA-specific IgG levels were measured using a commercial ELISA kit (Camillo Bioengineering Co., Ltd., Nanjing, China), following the manufacturer's instructions.

2.2.9. Serum cytokine and biochemical index detection

C57BL/6 male mice (20 ± 2 g) were subcutaneously immunized with two doses of OVA mRNA-loaded SAPC-LNPs, PC-LNPs, and 1.5PD-LNPs (10 μg/mouse) at a 14-day interval. Blood was collected from the orbital vein of mice 24 h after vaccination. To obtain mouse serum samples, the collected blood was placed at 4 °C overnight and centrifuged at 1000 g for 20 min. ELISA kits (Elabscience Biotechnology Co., Ltd) were used to detect interleukin-1β (IL-1β), interleukin-2 (IL-2), interleukin-6 (IL-6), and tumor necrosis factor-alpha (TNF-α) in mouse serum according to the protocol. Mouse serum in the 1.5 PD-LNPs group, PC-LNPs group, and SAPC-LNPs group was diluted by a factor of twenty for detection, while the control group's serum was diluted by a factor of two for detection. The final cytokine concentration is obtained by multiplying the measured value by the dilution factor. Glutamic oxaloacetic transaminase (AST), glutamic-pyruvic transaminase (ALT), creatinine (CRE), and blood urea nitrogen levels (BUN) were measured using test kits from Nanjing Jiancheng Bioengineering Research Institute according to their protocols.

2.2.10. Anti-PEG antibody detection

Serum levels of anti-PEG IgG and IgM were detected on day 7 after the first and second dose of mRNA vaccine, while anti-PEG IgE was detected 24 h after vaccination. 96-well plates were pre-coated with 1 μg PEGfilgrastim and sealed with 1 % BSA solution for 1 h. After washing the plates three times, diluted mouse serum was added to the wells and incubated at 37 °C for 1.5 h. Mouse serum was diluted by factors of 100, 20, and 10 times for measuring anti-PEG IgM, anti-PEG IgG, and anti-PEG IgE, respectively. After washing the plate 5 times, HRP-conjugated goat anti-mouse IgM (Invitrogen™) at a dilution of 1/2000, HRP-conjugated anti-mouse IgG (Invitrogen™) at a dilution of 1/

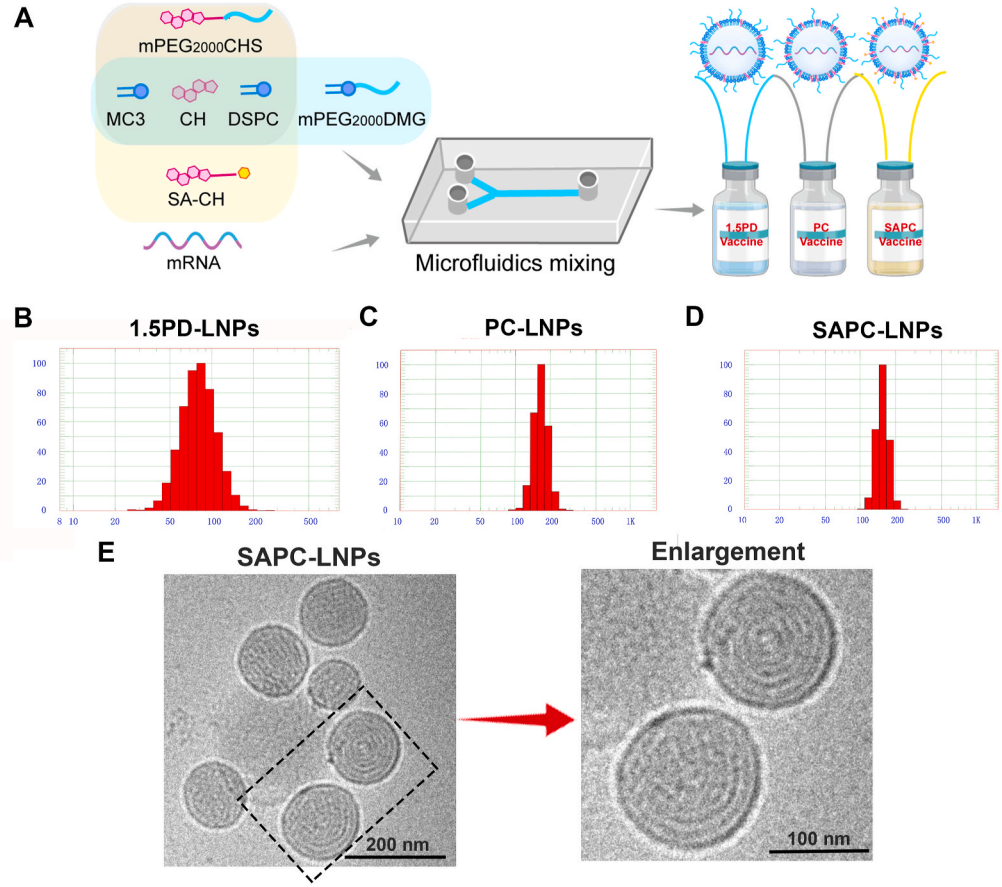

Fig. 1. Synthesis and characterization of mRNA LNPs. A) Flowchart of microfluidic hybrid synthesis of LNPs. Particle size distribution and preparation appearance of B) 1.5PD-LNPs C) PC-LNPs D) SAPC-LNPs. E) Cryo-TEM images of SAPC-LNPs, Scale bare = 200 nm. Cryo-TEM image at local magnification, Scale bare = 100 nm.

5000, and HRP-conjugated anti-mouse IgE (Invitrogen™) at a dilution of 1/1000 were added to the plates and incubated at 37 °C for 1 h each. Following another round of washing five times, color development was achieved using TMB for 15 min before being terminated with a solution containing sulfuric acid at a concentration of 1 mol/L. OD values were measured at wavelengths of both450 nm and630 nm using a multi-functional plate reader.

2.2.11. *Memory T cell detection*

For examination of memory T cells, spleens were collected from mice 7 days, 6 months, and 12 months after booster immunization. B16-OVA (3×10^5) tumor cells were inoculated into the right flank of the mice at these same time points, and spleens were also collected for T cell isolation seven days after tumor cell rechallenge. Single-cell suspensions were obtained by grinding the spleen and passing through 100-mesh strainers. Lymphocytes were separated using a mouse splenic lymphocyte separation solution (Haoyang Biological Products Technology Co., LTD, Tianjin, China) and centrifuged (450×*g*, 20 min) at room temperature to obtain the lymphocyte layer. Erythrocytes were lysed with 1 × RBC Lysis buffer (Invitrogen, 2376954), followed by termination with 1 × PBS and centrifugation (250×*g*, 10 min) at 4 °C. The cells were resuspended in PBS (1 × 106 cells/100 μL) and stained with Percp Cy5.5-*anti*-mouse CD3 (eBioscience™), FITC-*anti*-mouse CD8a (eBioscience™), PE-*anti*-mouse-CD44 (eBioscience™), and APC-*anti*-mouse-CD62L(eBioscienceTM) for 30 min at 4 °C in the dark. The stained cells were washed twice with PBS before being resuspended in a final volume of two hundred microliters of PBS for flow cytometry testing.

Table 1

Formulations	Particle size	PDI	*Zeta* potential (mV)	*EE*
PC-LNPs	161.4 ± 2.4	0.019 ± 0.008	0.20 ± 0.77	90.44 ± 0.52 %
SAPC-LNPs	145.8 ± 1.3	0.045 ± 0.024	2.20 ± 1.04	93.21 ± 0.90 %
1.5PD-LNPs	94.7 ± 2.2	0.165 ± 0.031	−4.20 ± 0.80	98.61 ± 0.18 %
SAPD-LNPs	153.4 ± 1.8	0.019 ± 0.011	0.30 ± 1.30	91.25 ± 0.53 %
0.2PD-LNPs	174.5 ± 2.0	0.029 ± 0.014	−2.80 ± 0.74	95.04 ± 0.34 %

2.2.12. *In vivo bioluminescence imaging*

For single dose injection detection, BALB/c mice (20 ± 2 g) were intramuscular injection (i.m.) with Fluc mRNA-loaded 1.5PD-LNPs, PC-LNPs, and SAPC-LNPs (10 μg/mouse, n = 3). For repeated injection detection, The first dose of Fluc mRNA-loaded 1.5PD-LNPs, PC-LNPs, and SAPC-LNPs (5 μg/mouse, n = 3). was pre-injected 5 days before, followed by a second injection (10 μg/mouse, n = 3). The mice were anesthetized with isoflurane. D-fluorescein potassium (3 mg/100 μL) was injected (i.p.) at 4, 8, 12, 24, and 48 h. In vivo bioluminescence imaging was performed 10 min later using a Xenogen IVIS Spectrum Imaging System (Perkin Elmer, USA). The luminescence intensity at each time point was calculated using Living Image (Perkin Elmer, USA) software.

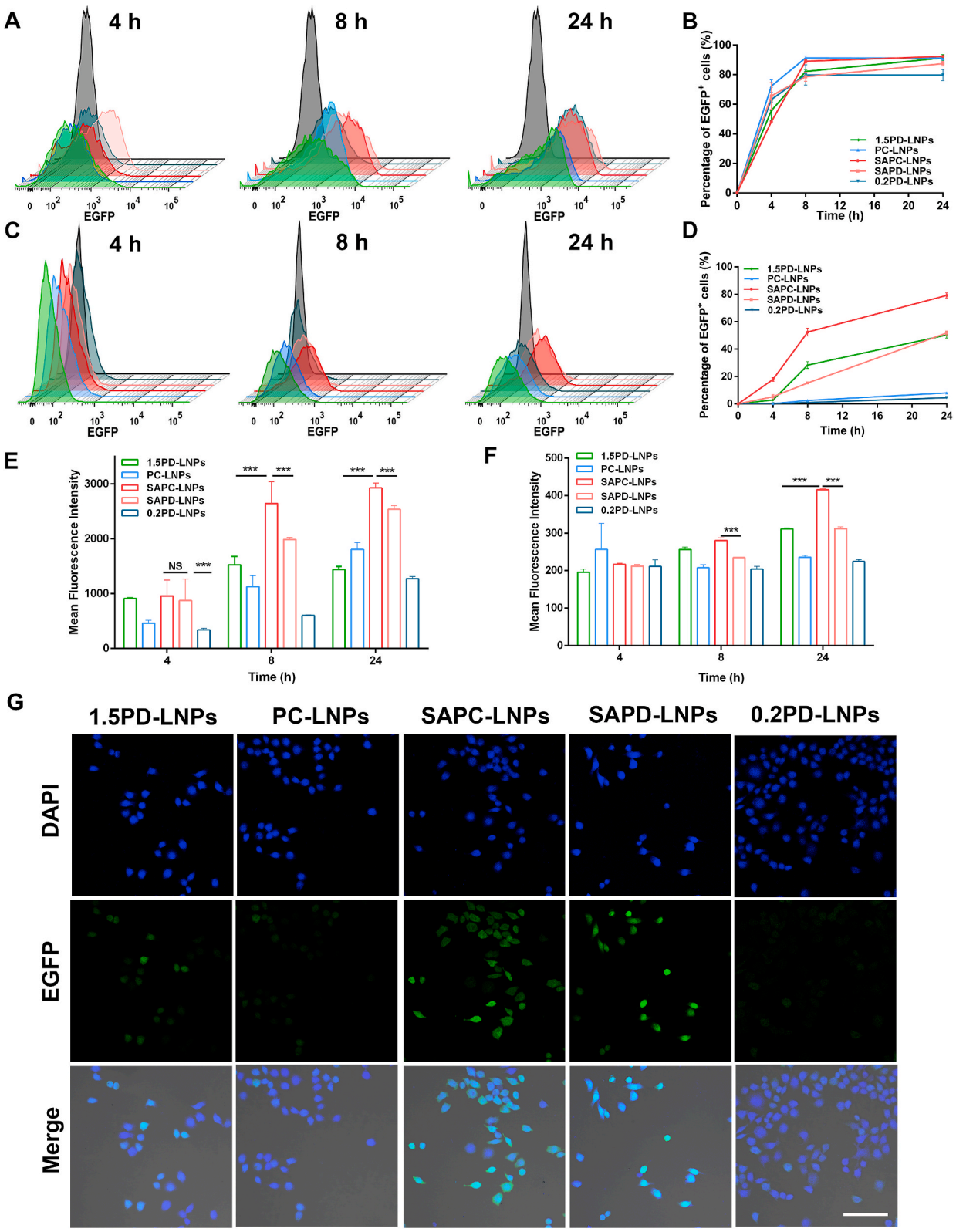

Fig. 2. Cellular transfection efficiency of different LNPs. (A) Histogram of mean fluorescence intensity, and (B) Percentage of EGFP positive DC2.4 cells incubated with 1.5PD-LNPs, PC-LNPs, SAPC-LNPs, SAPD-LNPs or 0.2PD-LNPs for 4 h, 8 h, and 24 h. (C) Histogram of mean fluorescence intensity, and (D) Percentage of EGFP positive RAW264.7 cells incubated with 1.5PD-LNPs, PC-LNPs, SAPC-LNPs, SAPD-LNPs or 0.2PD-LNPs for 4 h, 8 h, and 24 h. Mean fluorescence intensity of EGFP positive (E) DC2.4 cells, and (F) RAW264.7 cells determined by flow cytometry. Data were expressed as mean ± s.d. LSD posttest and one-way ANOVA were used for statistical analysis (*, $p < 0.05$; **, $p < 0.01$; ***, $p < 0.001$; ****, $p < 0.0001$). (G) Fluorescence imaging of DC2.4 cells after incubation with 1.5PD-LNPs, PC-LNPs, SAPC-LNPs, SAPD-LNPs or 0.2PD-LNPs for 24 h. Scale bar, 50 μm.

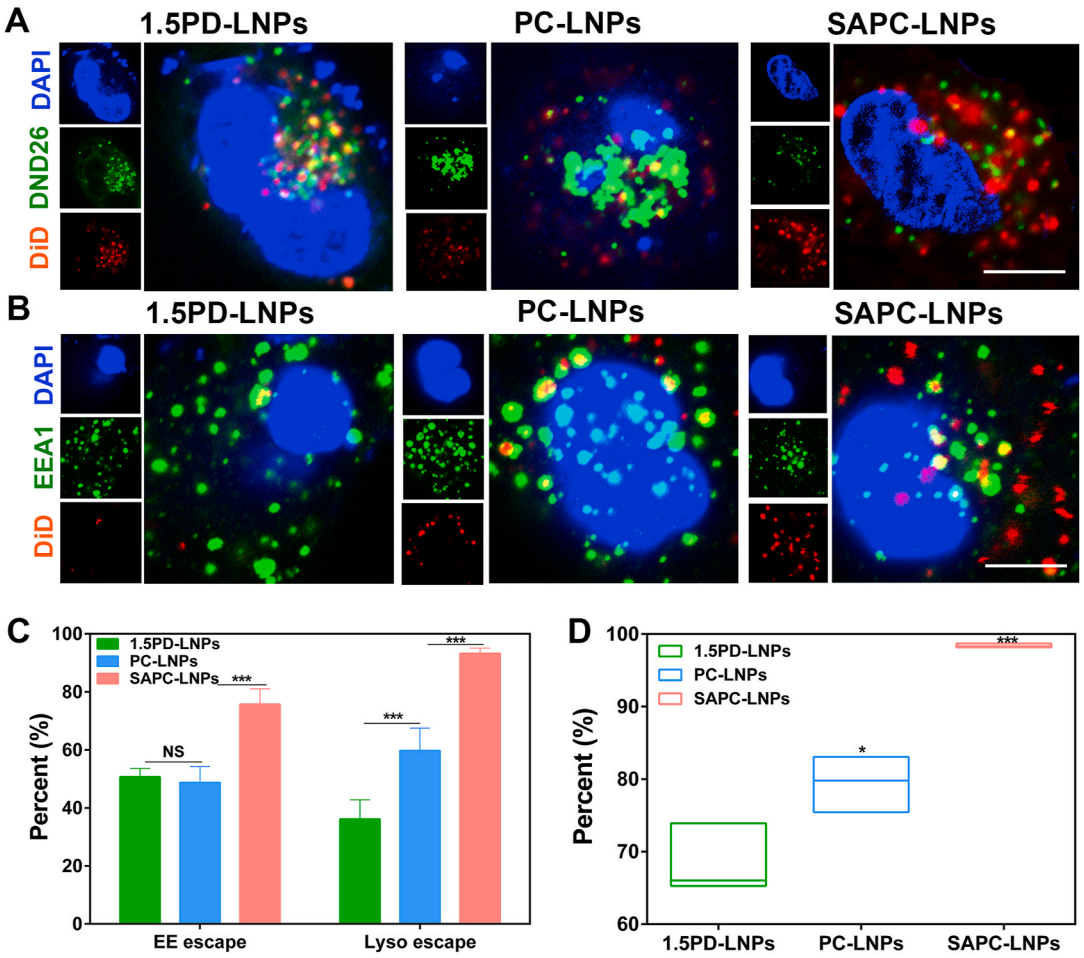

Fig. 3. Endosomes escape efficiency of different LNPs. Fluorescence images of (A) lysosome and (B) EE co-location with DiD-labeled 1.5PD-LNPs, PC-LNPs, and SAPC-LNPs in DC2.4 cells. Scale bars, 10 μm. (C) The EE and lysosome escape efficiency, and (D) total endosome escape efficiency of 1.5PD-LNPs, PC-LNPs, and SAPC-LNPs in DC2.4 cells. Data were expressed as mean ± s.d. LSD posttest and one-way ANOVA were used for statistical analysis (*, $p < 0.05$; **, $p < 0.01$; ***, $p < 0.001$; ****, $p < 0.0001$).

2.2.13. Statistical analysis

Statistical significance was determined by one-way ANOVA with LSD posttest using IBM SPSS Statistics software. A significant difference was defined as $P < 0.05$ with a 95 % confidence interval. Data are shown as mean ± s.d. Parallel experiments refer to multiple independent experiments. Animal experiments were performed randomly.

3. Results and discussion

3.1. Preparation and characterization of lipid nanoparticles

mRNA LNPs containing 1.5 mol% of $mPEG_{2000}DMG$ (1.5PD-LNPs), co-modified with SA-CH and cleavable $mPEG_{2000}CHS$ (SAPC-LNPs), or modified with cleavable mPEG2000CHS alone (PC-LNPs) were prepared by microfluidic mixing (Fig. 1A). The particle size, polydispersity index (PDI), Zeta potential, and encapsulation efficiency of LNPs encapsulated with EGFP mRNA are summarized in Table 1. The LNPs have a good appearance, and the particle size distribution is uniform (Fig. 1B–D). The structure of representative SAPC-LNPs was observed using frozen transmission electron microscopy. The LNPs in the field of view showed a uniform circular structure, and under local magnification, the electron-dense core region of LNPs exhibited a layered or fingerprint-like structure (Fig. 1E). The synthesis and characterization of SA-CH and $mPEG_{2000}CHS$ can be found in the supplementary information.

The desorption efficiency of PEG on $mPEG_{2000}CHS$-modified LNPs or $mPEG_{2000}DMG$-modified LNPs was measured in mouse serum at 37 °C, following the research method of Xu et al. [25]. The results showed that $mPEG_{2000}CHS$ could be cleaved by 60 % after being incubated with mouse serum at 37 °C for 12 h. However, the $mPEG_{2000}DMG$ could dissociate from the LNPs by only 16 %. Furthermore, $mPEG_{2000}CHS$--modified LNPs exhibited an almost four-fold increase in PEG dissociation (Fig. S1).

3.2. Cell transfection assay

We examined the transfection efficiency of various mRNA LNPs in dendritic cells (DCs) and macrophages, as these two types of cells are the main antigen-presenting cells (APCs) and abundantly express Siglec-1 [24–26]. DC2.4 cells and RAW264.7 cells were selected as the in vitro dendritic cell and macrophage models, respectively, for the expression of Siglec-1 on the surface of these cells (Fig. S2).

DC2.4 cells and RAW264.7 cells were selected as the in vitro models for dendritic cells and macrophages, respectively, due to their surface expression of Siglec-1 (Fig. S2). The in vitro transfection experiment showed that the percentage of EGFP + cells increased with prolonged incubation time. At 24 h, 80 % of RAW264.7 cells were transfected by SAPC-LNPs, while SAPD-LNPs and 1.5PD-LNPs only transfected 40 % of RAW264.7 at the same time points (Fig. 2C and D). Although there was no significant increase in the proportion of DC2.4 cells transfected by SAPC-LNPs at the same time points (Fig. 2A and B), the mean fluorescence intensity of EGFP-positive cells was 1.5-fold and 2-fold higher than that of PC-LNPs and 1.5PD-LNPs group respectively when treated

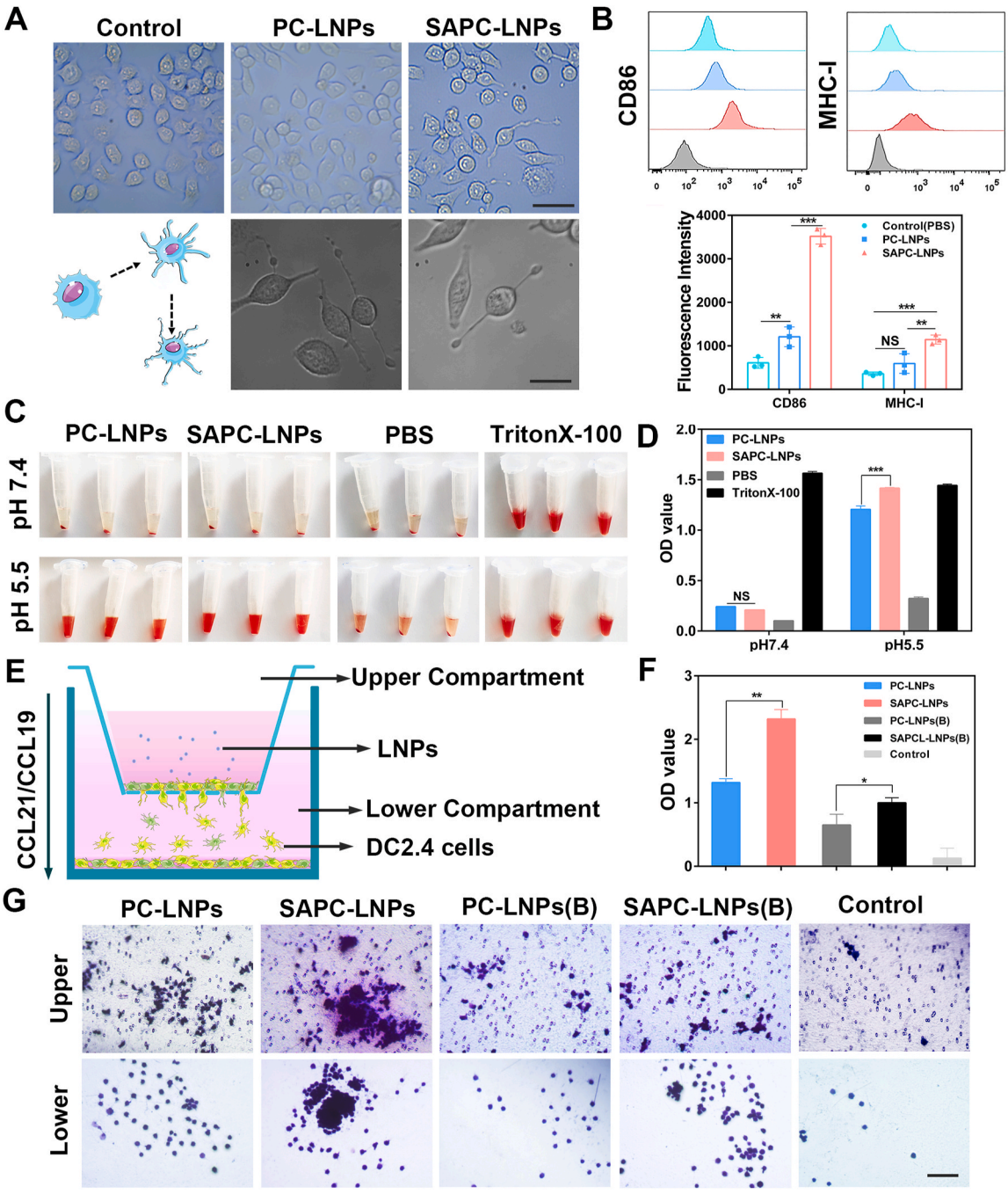

Fig. 4. SA-modified LNPs promote the maturation and migration of DCs. (A) DC2.4 cells with different morphology, and (B) CD86, MHC-I expression after incubation with OVA mRNA-loaded SAPC-LNPs or PC-LNPs (mRNA, 1 μg/mL) for 24 h. DCs in the visual field are divided into mature DCs (mDCs), semi-mature DCs (semi-mDCs), and immature DCs (imDCs). Scale bars, 20 μm. The fusion ability of different LNPs to endosome membrane under different pH conditions was evaluated in vitro by using 4 % RBC. The (C) images and (D) OD values after different LNPs incubated with 4%RBC reflected the ability of LNPs fusing with the endosome membrane. (E) The protocol of transwell experiments. OVA mRNA-loaded SAPC-LNPs, PC-LNPs (1 μg/mL), and an equivalent volume of blank PC-LNPs and SAPC-LNP were added to the transwell upper chamber with CCL19 (250 ng/mL), CCL21 (250 ng/mL) added to the lower chamber (n = 3) and co-incubated for 24 h. (F) The migrating cells were decolorized with 20 % acetic acid and the OD values were read. Data were expressed as mean ± s.d. LSD posttest and one-way ANOVA were used for statistical analysis. (G) Crystal violet-stained migrating DC2.4 cells were imaged under an inverted microscope. Scale bar, 50 μm. (For interpretation of the references to colour in this figure legend, the reader is referred to the Web version of this article.)

with SAPC-LNPs (Fig. 2E and F). The use of confocal laser microscopy (CLSM) also confirmed that SAPC-LNPs efficiently transfect DCs since DC2.4 cells treated with SAPC-LNPs exhibited significantly bright green fluorescence (Figure G), which was consistent with flow cytometry results.The results indicated that SA-modified LNPs can efficiently transfect APCs, thereby facilitating more APCs to acquire antigens for presentation to T lymphocytes. Moreover, we also found that the transfection efficiency of APCs was better when SA was co-modified with cleavable PEG lipids compared to LNPs co-modified with $mPEG_{2000}DMG$.

3.3. SA-modified LNPs accelerate endosome escape

Endosome escape is essential for mRNA delivery. The function of

ionizable lipids in LNPs is to disrupt the endosome membrane, promoting mRNA release into the cytoplasm and facilitating complete translation. However, structural optimization of ionizable lipids cannot simultaneously enhance both cellular uptake and endosomal escape efficiency of LNPs [12]. The SAPC-LNPs not only enhanced cellular uptake efficiency but also rapidly escaped early endosomes (EEs) and lysosomes. After incubating DiD-labeled SAPC-LNPs with DC2.4 cells for 2 h, it was observed that the intensity of red fluorescence in DC2.4 cells was up to 2 times higher than that of PC-LNPs and 1.5PD-LNPs. At 2 h, the escape rate of SAPC-LNPs from EEs reached up to 80 %, while PC-LNPs and 1.5PD-LNPs had escape rates of only 50 %. Additionally, the lysosome escape rate of SAPC-LNPs was as high as 90 %, whereas PC-LNPs and 1.5PD-LNPs had lysosome escape rates ranging from only 40 %–60 % (Fig. 3C). Only ten green dots can be observed in one cell in the SAPC-LNPs group, whereas there were numerous green fluorescent dots present in one cell of the other groups (Fig. 3A). Image J software was utilized to quantify the overall lysosome area in the images. The results revealed that the total lysosome area in SAPC-LNPs was significantly lower compared to our groups, indicating a significant reduction in the number of lysosomes within cells incubated with SAPC-LNPs when compared to the other two groups (Fig. S3). In addition, the lysosomes of cells in the 1.5PD-LNPs and PC-LNPs groups were mainly distributed near the nucleus, and these lysosomes in this region were secondary lysosomes with strong digestive ability. On the other hand, the lysosomes of cells in the SAPC-LNPs group were primary lysosomes, they were primarily located at the cell edge, which had weak digestion ability (Fig. 3A and B).

The LNPs uptake by cells enter into EE firstly, and the LNPs that failed to escape from EE will be further transported to the lysosomes, where part of the LNPs can still escape. Therefore, evaluating the escape efficiency of the LNPs merely in a particular stage of the endosome pathway in cellular cannot comprehensively represent the total endosome escape rate. To comprehensively evaluate the escape efficiency of different LNPs at different endosome stages, the following formula was used to calculate the total cellular endosome escape efficiency:

$$\text{Total endosome escape efficiency (teE)} = \text{eEE} + (100\% - \text{eEE}) \times \text{eLyso}$$

eLyso: escape efficiency of lysosomes; eEE: escape efficiency of early endosome

The results showed that the transfection efficiency (teE) of SAPC-LNPs was almost 100 % (98.40 ± 0.22 %), while the teE of PC-LNPs and 1.5PD-LNPs was only 80 % and 70 %, respectively. The substantial improvement in the transfection efficiency of SAPC-LNPs in APCs is related to both DC-targeting and accelerated endosome escape by SA. Most importantly, we found that the SAPC-LNPs simultaneously improved both cellular uptake and total endosome escape efficiency, which was not reported in other studies, as an increase in endosome escape rate sometimes accompanied a decrease in cellular uptake effect [12].

Interestingly, according to previous research, only 1–2% of RNA payloads can finally escape from the lysosomal to the cytosol via LNPs [27]. However, in our study, the lysosome escape rate of SAPC-LNPs was as high as 90 %. There may be several reasons for these different results. Firstly, we have observed that SA-modified LNPs show extremely low colocalization with lysosomes in the DCs. Currently, we haven't figured out a way to detect whether the SAPC-LNPs quickly escaped from the lysosomes or did not enter them at all. It is probable that SA-modified LNPs evade lysosomal pathways through some unknown mechanism which we will continue to explore in future studies. Secondly, Cy5-labeled RNA is commonly used for studying lysosome escape efficiency, which differs from the DiD-labeled LNPs used in our experiment. However, currently labeling both LNPs and mRNA has its own rationale and limitations.

DiD is easily synthesized with high purity, and the DiD-labeled LNPs can reflect the intracellular localization of LNPs. The structure of DiD shows that it has two C18 chains, which are similar to DSPC (one of the components of LNPs). This indicates that fluorescence probes such as DiD label the lipid membranes of LNPs with a firm binding and have less impact on the structure of LNPs. However, one limitation is that the DiD-labeled LNPs cannot reflect the release behavior of mRNA in cells. Although Cy5-labeled mRNA can reflect the release behavior of mRNA in cells, mRNA is fragile and easily broken. Any uncontrolled breakage of mRNA will affect the fluorescence intensity during detection, resulting in a low quantitative value. Additionally, the esterase catalyzes the cleavage of the ester bond between Cy5 and mRNA in the lysosome, resulting in a detected fluorescence signal that is not necessarily RNA but may be the free form of Cy5. Some mRNA molecules escaping from the lysosome may not be detected due to the loss of fluorescent labeling. Furthermore, most fluorescent probes are hydrophobic, and their coupling with mRNA reduces its hydrophilicity, leading to changes in both the structure of LNPs prepared by fluorescent-labeled mRNA and the release behavior of RNA. Specifically, currently prepared Cy5-labeled mRNA is transcribed in vitro using Cy5-coupled UTP, which means an mRNA molecule may contain dozens to hundreds of Cy5-UTP molecules that can greatly impact the physicochemical properties of mRNA. It should also be noted that mRNA does not necessarily escape from the lysosome as a single molecule; instead, some parts of it may escape by binding with lipids. Additionally, it needs to be determined whether the fluorescence signal from fluorescence probe-labeled mRNA wrapped inside LNPs is strong enough to reach the detection limit of instruments. Therefore, a low detection value may result when using a lysosome escape assay with fluorescence probe-labeled mRNA. More scientific labeling methods need to be developed perhaps by simultaneously labeling LNPs and mRNA to establish more scientifically valid evaluation indices for assessing endosome escape efficiency in future studies.

3.4. SA-modified LNPs promote the maturation and migration of DCs

Immature DCs (imDCs) and semi-mature DCs (semi-mDCs) can lead to immune tolerance, while only fully mature DCs (mDCs) can effectively activate naïve T cells and generate strong anti-tumor immune responses [28,29]. The morphology of DCs changed significantly after being incubated with SAPC-LNPs for 24 h. A special morphology characterized by long protrusions and microbead-like structures was observed in SAPC-LNPs treated DCs. However, no microbeads were observed on the protrusions of DCs treated with PC-LNPs at an equal mRNA concentration (Fig. 4A). Flow cytometry analysis revealed a significant upregulation of CD86 and MHC-I expression levels (Fig. 4B), further confirming that SA-modified mRNA LNPs-treated DCs exhibited higher maturity.

The SAPC-LNPs have greater lysosomal membrane destructive ability in acidic environments, which leads to further release of mRNA and MHC-I from the lysosomes into the cytoplasm, also explaining why SAPC-LNPs treated cells produce fewer lysosomes at the same incubation time. The erythrocyte membrane was used as a simulation for lysosomes at a concentration of 4 %. The hemolysis capacity of SAPC-LNPs was significantly higher than that of PC-LNPs at pH 5.5, which is similar to that in lysosomes. However, under physiological conditions (as shown in Fig. 4C and D), neither PC-LNPs nor SAPC-LNPs caused any hemolysis. These results indicate that SA-modified LNPs are safe under physiological conditions but can induce rupture of lysosomal membranes in an acidic environment. The addition of SA changes the lipids distribution in the outer layer of LNPs; more ionizable lipids migrate from the core of LNPs to the outer layer, making LNPs carry more positive charge under acidic conditions and accelerating lysosome escape. Besides, SA modification promoted DCs migration by transwell experiment (Fig. 4E), which was reflected in SAPC-LNPs loaded with or without mRNA (Fig. 4F). In summary, SA-modified LNPs enhance both maturation and migration of DCs, thereby facilitating antigen presentation to T cells and promoting memory T cell formation.

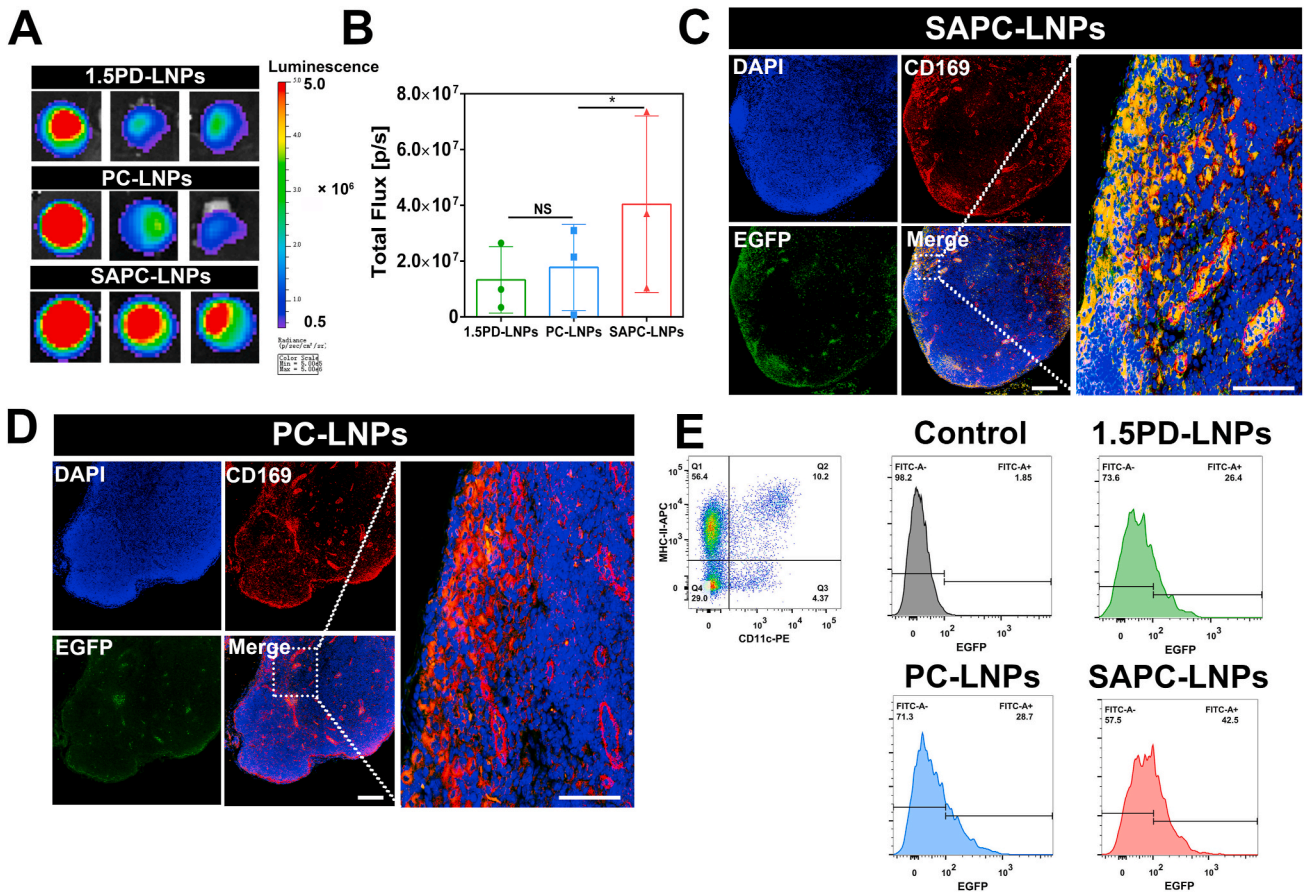

Fig. 5. SA modification enhance the targeting ability of LNPs. (A) Images, and (B) quantitative analysis of bioluminescence imaging of lymph nodes at 24 h after subcutaneously injected Fluc mRNA encapsulated 1.5PD-LNPs, PC-LNPs, and SAPC-LNPs. Immunofluorescence imaging of mouse lymph nodes of EGFP mRNA encapsulated (C) SAPC-LNPs, and (D) PC-LNPs. Scale bars = 100 μm. (E) Flow analysis of EGFP positive DCs in lymph nodes. The $CD11c^{+}MHC\text{-}II^{+}$ population represent DCs.

3.5. SA-modified LNPs target dendritic cells in lymph nodes

Since the mRNA LNPs injected subcutaneously may be enriched in nearby lymph nodes, we further studied the lymph node targeting ability of SA-modified LNPs in vivo. We observed that 24 h after subcutaneous injection, the Fluc expression level in popliteal lymph nodes of the SAPC-LNPs group was significantly higher than that in other groups (Fig. 5A and B). Further analysis revealed that SAPC-LNPs primarily transfected cells with high expression of CD169 (a type of SA receptor) in lymph nodes. $CD169^{+}$ cells in popliteal lymph nodes of mice injected with SAPC-LNPs exhibited higher levels of EGFP compared to those in the PC-LNPs group (Fig. 5C and D). Mononuclear cells from mice's popliteal lymph node were isolated and analyzed for the proportion of $EGFP^{+}$DCs using flow cytometry. The results demonstrated that $EGFP^{+}$DCs accounted for up to 42.5 % in the SAPC-LNPs group, which was twice as much as that observed in both the 1.5PD-LNPs group and PC-LNPs group (Fig. 5E). In conclusion, SA-modified LNPs can effectively target DCs located near the injection site within lymph nodes and efficiently translate mRNA encoding proteins within these DCs.

3.6. SA-modified LNPs produce robust immune memory to antigen and low side effect

The tumor prevention effects of different mRNA vaccines were tested using the protocol described in Fig. 5A. The incidence of side effects of the Pfizer-BioNTech COVID-19 mRNA vaccine is 80–90 %, and severe side effects can reach 10 % [30,31]. The weight changes in the mice were monitored to assess safety. Approximately 5 % of body weight was lost after the first vaccination (Fig. 6B–G). After the second dose, the mean body weight of mice treated with 1.5PD-LNPs decreased by 10 %, and within 24 h, 25 % of the mice lost 15 % of their body weight (Fig. 6I). However, the weight loss in other groups was less than 5 % (Figure J–N), especially in the SAPC-LNPs group where there was no significant difference compared to the control group after the second vaccination. Similar to our observations, people tend to experience more severe side effects after receiving a second dose of SARS-Cov-2 mRNA vaccines [32].

The time from weight loss to recovery of mice after vaccination varied, and the duration of the recovery period also reflected the side effects of different vaccines. Therefore, evaluating the side effects of vaccines solely based on the percentage change in body weight is not accurate. To further assess the safety of different mRNA vaccines, we calculated the area above the curve (AAC) for the percentage change in body weight in mice vaccinated with various vaccines after 7 days. After the first vaccination, there was no significant difference observed in AAC for body weight change among all groups of mice (Fig. 6H). However, after the second vaccination, AAC for percentage change in body weight was twice as high in mice administered with 1.5PD-LNPs compared to those given SAPC-LNPs and showed no significant difference from that of control group (Fig. 6O). This suggests that commercially formulated mRNA vaccines caused severe side effects in mice while SA-modified mRNA vaccine significantly reduced these side effects. The reduction in side effects may be attributed to using cleavable $mPEG_{2000}CHS$ since it has been reported that PEG_{2000}-lipid conjugate could contribute to allergic reactions associated with SARS-Cov-2 mRNA vaccines rather than native PEG [33].

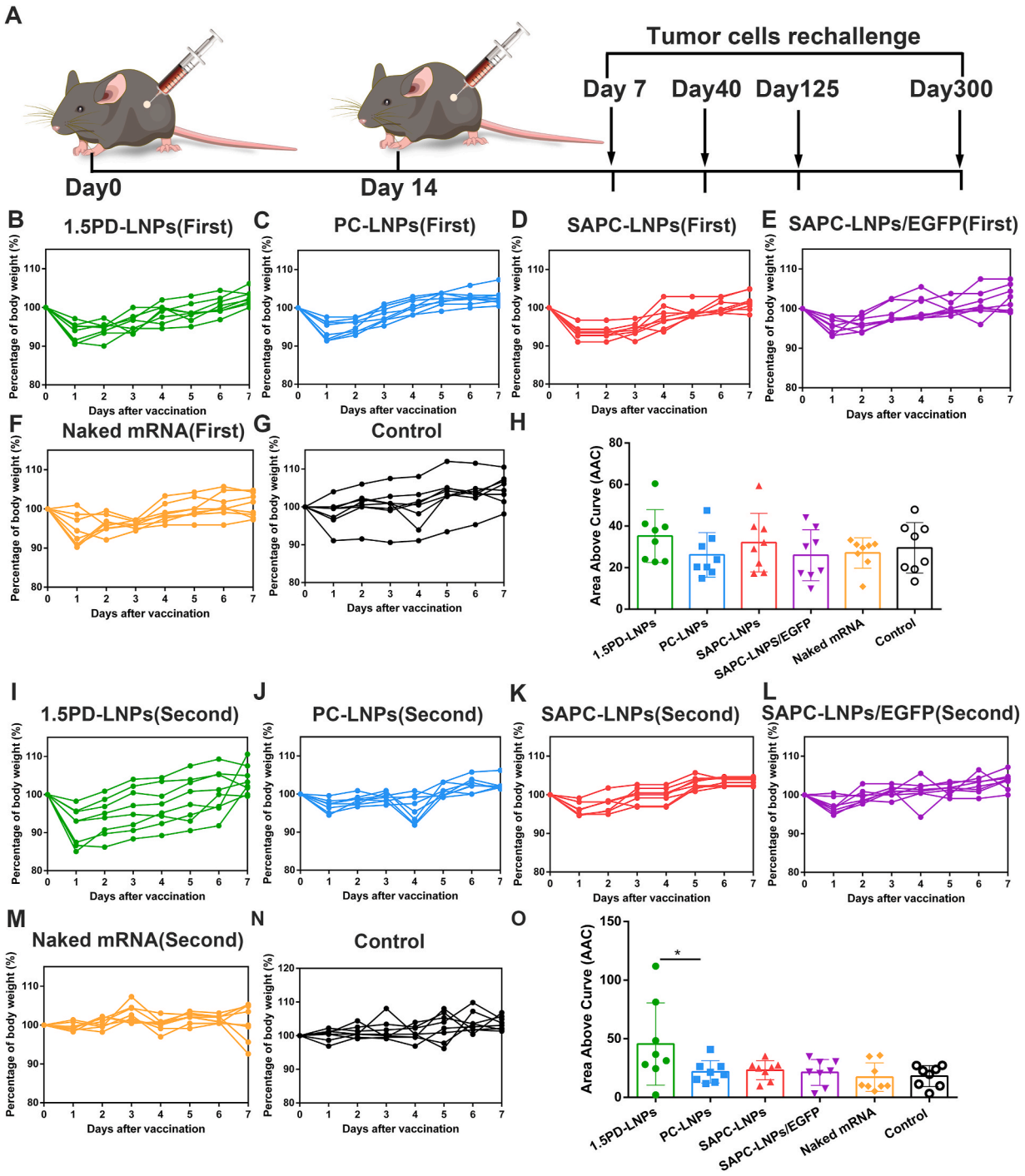

Fig. 6. The SA-modified vaccine showed lower side effects. (A) Vaccination schedule. mRNA vaccines were administrated subcutaneously (10 μg/mouse) twice at 14 days intervals. B16-OVA cells were rechallenged on days 7, 40, 125, and 300 after booster immunization. The percentage of weight change in mice within 7 days after initial vaccination of (B) 1.5PD-LNPs, (C) PC-LNPs, (D) SAPC-LNPs, (E) SAPC-LNPs/EGFP mRNA, (F) naked OVA mRNA, and (G) control. (H) AAC of the weight change curve in each group after the first vaccination. Data were expressed as mean ± s.d (n = 8). The percentage of weight change in mice within 7 days after the second vaccination of (I) 1.5PD-LNPs, (J) PC-LNPs, (K) SAPC-LNPs, (L) SAPC-LNPs/EGFP mRNA, (M) naked OVA mRNA, and (N) control. (O) AAC of the weight change curve in each group after the second vaccination. Data were expressed as mean ± s.d (n = 8).

The reported cases of hypocomplementemic urticarial vasculitis following SARS-CoV-2 mRNA vaccination have been associated with amplification of TNF-α, IL-1, and IL-6 [34]. We hypothesized that the significant weight loss observed in mice from the 1.5PD-LNPs group may be related to changes in inflammatory cytokine levels. Therefore, we examined the serum inflammatory cytokines of mice after the first and second vaccinations. Experimental results revealed a significant increase in inflammatory cytokine levels after the second injection of each mRNA vaccine. However, compared to the first injection 24 h later, the mRNA vaccine prepared according to the commercial formula showed an increase of 1~3 times higher levels, which was significantly greater than those observed in PC-LNPs and SAPC-LNPs groups. Notably, IL-6 levels reached as high as 2000 pg/mL at 24 h after the second injection in the serum of mice from the 1.5PD-LNPs group (Fig. 7A–D). Additionally, various blood biochemical indexes were measured for mice, showing a significant reduction in serum AST levels for those from the 1.5PD-LNPs

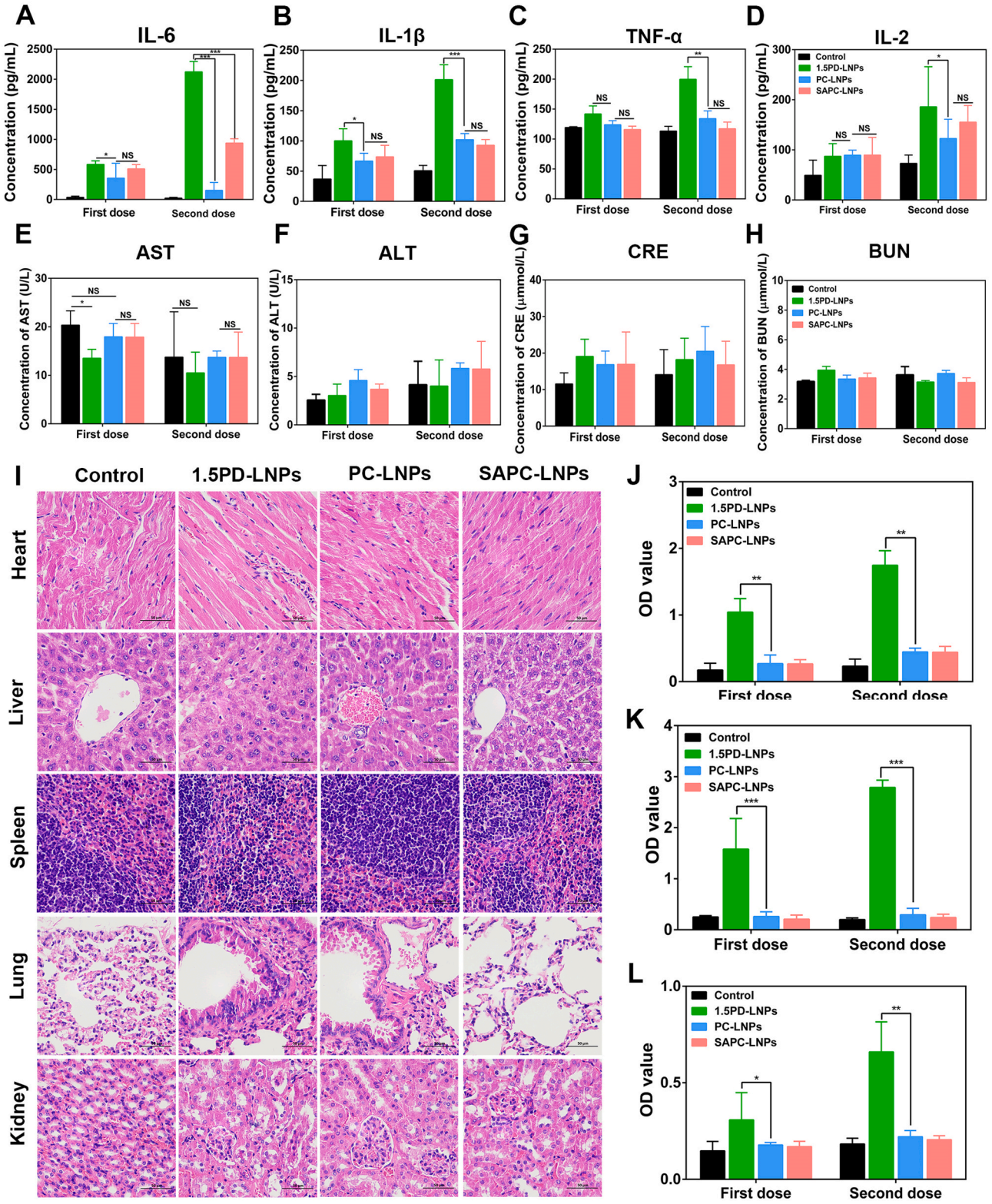

Fig. 7. Safety assessment of LNPs with different mRNA LNPs. Serum concentrations of (A) IL-6, (B) IL-1β, (C) TNF-α, (D) IL-2, (E) AST, (F) ALT, (G) CRE, (H) BUN were determined after initial and repeated injection of different mRNA LNPs. (I) H&E staining of major organs, scale bars = 50 μm. Level of (J) anti-PEG IgM, (K) anti-PEG IgG, and (L) anti-PEG IgE in serum after first and second injection of different mRNA LNPs. LSD posttest and one-way ANOVA were used for statistical analysis (*, $p < 0.05$; **, $p < 0.01$; ***, $p < 0.001$).

group; no other notable abnormalities were observed among other biochemical indexes (Fig. 7E–H). H&E staining results for major organs indicated that none of these mRNA LNPs caused significant tissue damage after their second injection (Fig. 7I).

Studies have suggested that the side effects of mRNA vaccines are related to anti-PEG antibodies [35,36], and we detected anti-PEG antibodies in mouse serum using ELISA. The levels of anti-PEG IgG and IgM in the 1.5PD-LNPs group were significantly higher than those in the

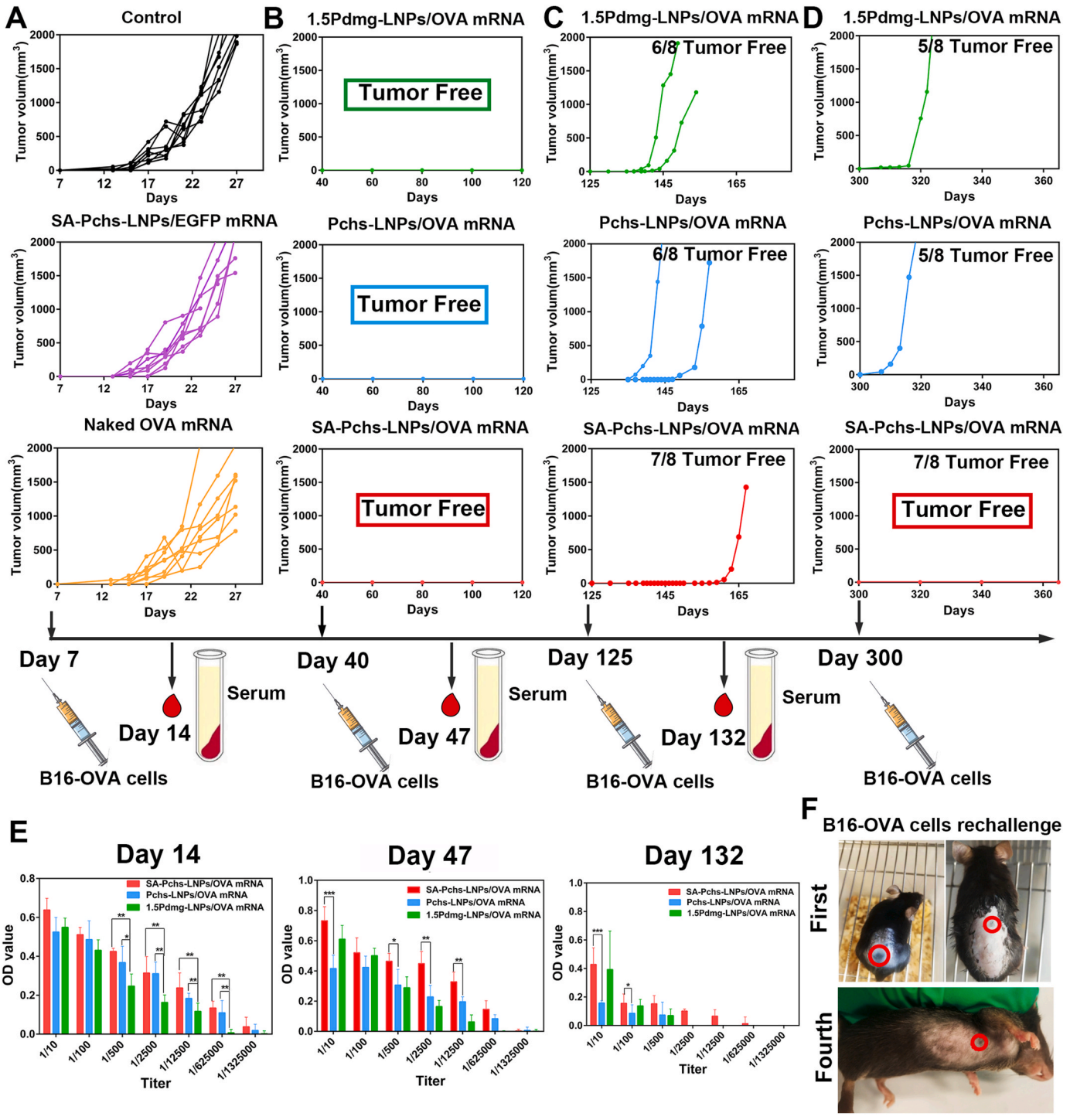

Fig. 8. The SA-modified vaccine has more durable preventive protection. (A) The tumor growth curves of mice in control, SAPC/EGFP and naked mRNA group after the first tumor cells rechallenge at day 7–30. (B) The tumor growth curves of mice in 1.5PD-LNPs, PC-LNPs, and SAPC-LNPs after the second tumor cells rechallenge at day 40–120. (C) The tumor growth curves of mice in 1.5PD-LNPs, PC-LNPs, and SAPC-LNPs after the third tumor cells rechallenge at day 125–180. (D) The tumor growth curves of mice in 1.5PD-LNPs, PC-LNPs, and SAPC-LNPs after the fourth tumor cells rechallenge at day 300–360. (E) Antibody titers on day 14, day 47, and day 132 after booster immunization. (F) Several mice vaccinated with 1.5PD-LNP showed black plaques, which were photographed before they faded. LSD posttest and one-way ANOVA were used for statistical analysis (*, $p < 0.05$; **, $p < 0.01$; ***, $p < 0.001$).

PC-LNPs and SAPC-LNPs groups (Fig. 7J and. K). Unlike anti-PEG IgM and anti-PEG IgG, almost no detectable levels of anti-PEG IgE were found in the serum of each group at day 7 after the second injection. However, we observed a significant increase in induced anti-PEG IgE at 24 h after the second injection., while only slight levels of anti-PEG IgE were detected in the PC-LNPs and SAPC-LNPs groups after the second injection (Fig. 7L). Although it is unclear whether the level of anti-PEG IgE reached concentrations capable of triggering an allergic reaction in mice tested, no symptoms of anaphylaxis were observed in mice vaccinated with each mRNA vaccine. Nevertheless, there was a dramatic reduction in body weight among mice in the 1.5PD-LNPs group suggesting that production of anti-PEG IgE is related to side effects caused by commercially formulated vaccines. It should be noted that SAPC-LNPs did not induce a strong immune response against PEG after

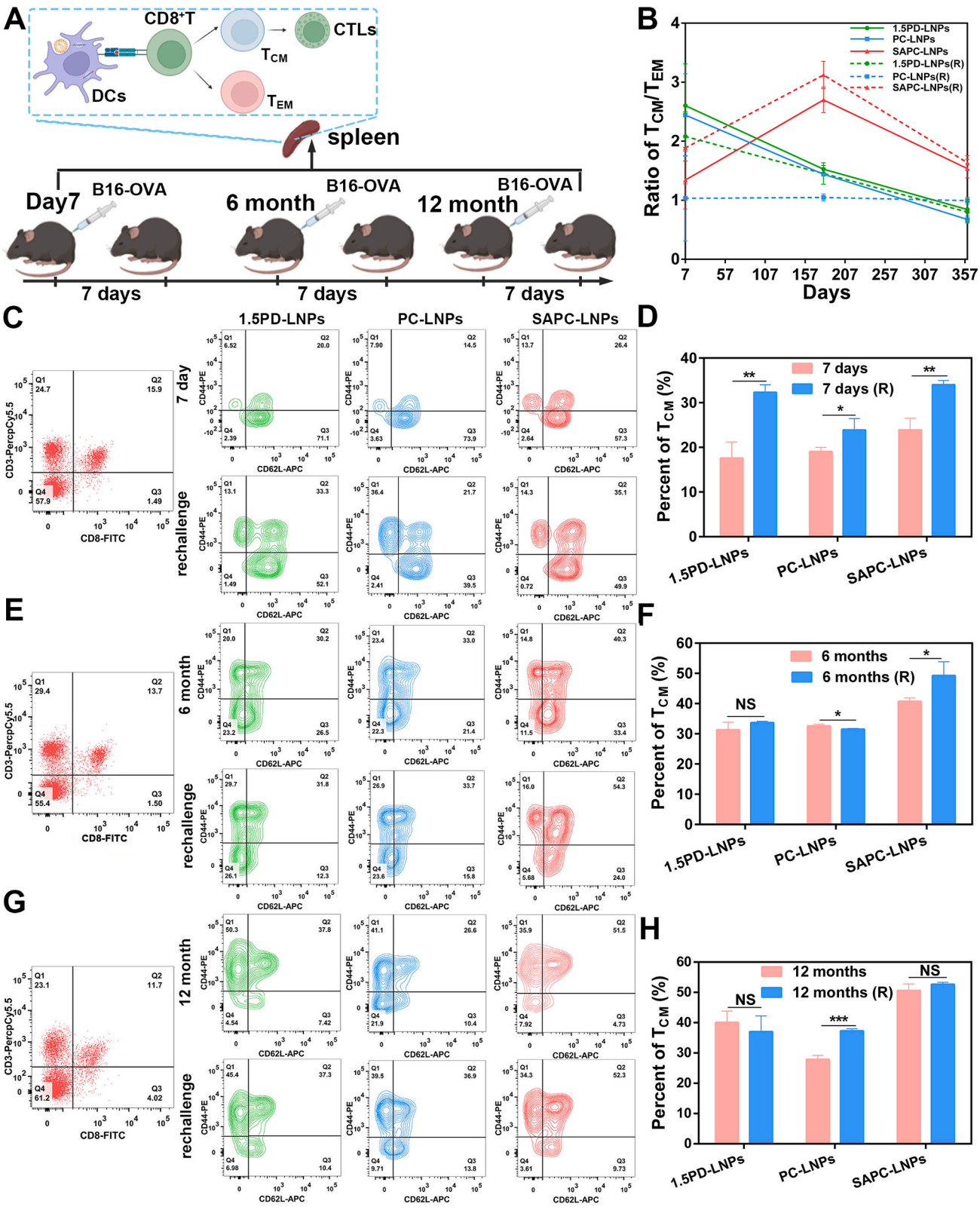

Fig. 9. Immune memory after vaccination. (A) Flow chart of differentiation and detection of memory T cells. (B) The ratio of T_{CM}/T_{EM} at different time points after the second vaccination with different LNPs. The percentage of mice splenic T_{CM} and T_{EM} before or after tumor cells rechallenge at (C, D) 7 days, (E, F) 6 months, and (G, H) 12 months. Data were expressed as mean ± s.d (n = 3). LSD posttest and one-way ANOVA were used for statistical analysis (*, $p < 0.05$; **, $p < 0.01$; ***, $p < 0.001$).

the second injection, indicating that there was weak memory within immune system towards SAPC-LNP vector itself.

The protective efficacy of different vaccines was studied by inoculating tumor cells into immunized mice multiple times. At 7 days after the second vaccination, 3×10^5 B16-OVA cells were injected into the mice. All the mice vaccinated with mRNA LNPs achieved 100 % protection, while all of the mice injected with SAPC-LNPs/EGFP mRNA and naked mRNA showed tumor growth (Fig. 8A). A second tumor cell rechallenge was performed at day 40 after booster immunization, and the different LNPs still provided a 100 % protection rate (Fig. 8B). The third tumor cell rechallenge occurred on day 125 after the second vaccination. At this time, the preventive protection rate of PC-LNPs and 1.5PD-LNPs decreased to 75 %, while the preventive protection rate of SAPC-LNPs remained close to 90 %, with only one mouse in the SAPC-LNPs group showing tumor growth after 20 days of rechallenge. The rate of tumor growth was significantly slower than that in the other two prevention groups (Fig. 8C). The fourth tumor cell rechallenge took place on day 300 after the second vaccination, and the preventive protection rate of PC-LNPs and 1.5PD-LNPs decreased to 62.5 %. However, prophylactic protection using SAPC-LNPs remained at 87.5 %, with no observed tumor growth even 60 days after rechallenging (Fig. 8D). Additionally, the black plaques appeared on the skin of mice in the 1.5PD-LNPs group, but they gradually faded (Fig. 8F), suggesting that a 75 % protection rate provided by 1 0.5 PD -LNPs may not be sufficiently conservative.

The long-lasting protective efficacy of vaccines is closely related to the formation of immune memory. The stronger the immune memory, the more durable protection produced by the vaccine. However, it is not clear which immune cell dominates anti-tumor immune memory. We tested serum levels of anti-OVA IgG in mice after three rounds of rechallenges, and the SAPC-LNPs group had the highest level of antibodies. However, after three rounds of tumor cell rechallenge, anti-OVA IgG levels had decreased to 30 % of the initial level (Fig. 8E). Interestingly, after the third tumor cell rechallenge, SAPC-LNPs-inoculated mice were still able to maintain a protection rate of 87.5 %, which may be related to the formation of memory T cells. The continuous activation of central memory T cells (T_{CM}) is necessary for maintaining anti-tumor immunity38. Therefore, we analyzed the proportion of T_{CM} before and after tumor cell rechallenge according to Fig. 9A protocol. The proportion of T_{CM} in mice from both SAPC-LNPs and 1.5PD-LNPs groups showed no significant difference on day 7 after booster immunization. After tumor cell rechallenge, there was a significant increase in TCM proportion among mice that received two doses of vaccine; however, there was no significant difference between SAPC-LNPs and 1.5PD-LNPs groups (Fig. 9C and D). The percentage of T_{CM} in mice from SAPC-LNPs group increased to 40 % at six months post-vaccination and continued growing to 54.6 % on day seven following subsequent tumor cell rechallenge (Fig. 9E and F). On the other hand, the percentage remained at only 30 % for mice from both 1.5PD-LNPs and PC-LNPs groups with no significant increase observed after tumor cell rechallenge (Fig. 9E and F). The proportion of T_{CM} of mice from SAPC-LNPs group remained above 50 %, while the level of T_{CM} in the other two groups was only 30 % at 12 months after vaccination (Fig. 9G and H). T_{CM} is a type of memory T cells with long-term memory that is generated by antigen-stimulated naïve T cells and can home to lymphoid tissue to receive repeated stimulation by antigens. Effective memory T cells (T_{EM}) can be directly generated by T_{CM} when antigens attack again, circulating throughout the body via blood and lymph fluid. However, we found that the T_{EM} ($CD3^+CD8^+CD44^+CD62L^-$) accumulation in the spleen increased significantly as the mice aged. At 12 months after vaccination, the level of T_{EM} in the spleen of mice in 1.5PD-LNPs group was up to 50 %, and a large quantity of T_{EM} occupied the compartments of T_{CM}, resulting in the number of T_{CM} decreased. Therefore, we calculated the spleen T_{CM}/T_{EM} ratio to assess the long-lasting effectiveness of immune memory formation after different vaccinations and found that the T_{CM}/T_{EM} ratio in the 1.5PD-LNPs and PC-LNPs groups decreased continuously from day 7 to month 12 after booster vaccination, dropping even below 1 (Fig. 9B). The T_{CM}/T_{EM} ratio in the SAPC-LNPs group increased during the first 6 months but decreased from month 6 to month 12; however, its value remained more than twice that of the other two groups (Fig. 9B). These results reasonably explain why SAPC-LNPs have a durable preventive protective effect. The promotion of TCM formation by SAPC-LNPs may be related to SA targeting DCs. It has been reported that DCs are the only type of APCs capable of activating naïve T cells, and T_{CM} is precisely generated by naïve T cells upon receiving antigen stimulation.

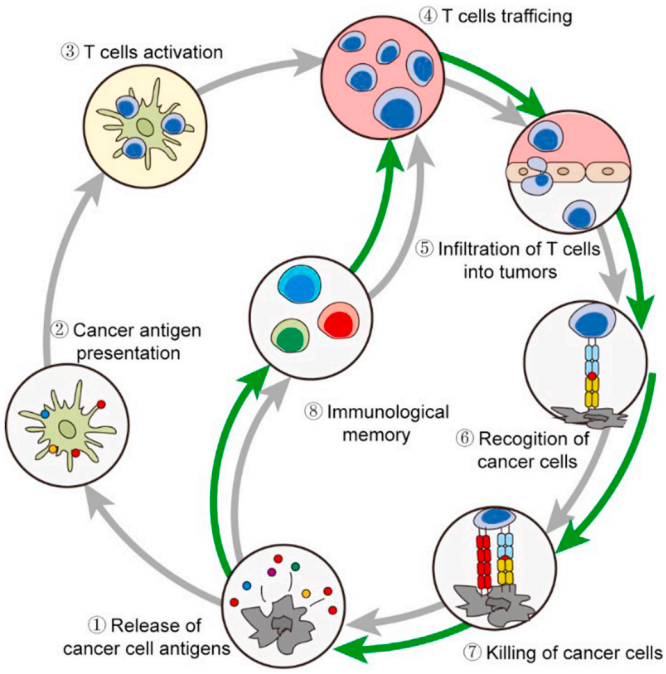

Fig. 10. New conceptual map of tumor immune cycle. The anti-tumor immunity is accomplished by an 8-step immune event. Step ①, the antigen released by the tumor cells; Step ②, tumor antigen presentation; Step ③, T cells activation; Step ④, T cells trafficking; Step ⑤, T cells infiltrated into tumors; Step ⑥, T cells recognize tumor cells; Step ⑦, T cells kill tumor cells; Step ⑧, immune memory formed. The memory T cells can be activated directly to produce effector T cells upon re-exposure to the tumor antigen. The whole tumor immune cycle is divided into a large cycle and a small cycle. The large circle is involved in the step ①②③④⑤⑥⑦⑧①, and the small circle is involved in the step ①⑧④⑤⑥①.

Another thing worth discussing is that black plaques appeared on the skin of mice in 1.5PD-LNPs and gradually faded away. The number of memory T cells generated is insufficient to combat invading tumor cells upon rechallenge, resulting in gradual tumor growth and the development of black plaques. However, with the initiation of the anti-tumor immune cycle, new memory T cells are generated and mobilized to produce effector T cells, which completely eradicate the tumor, leading to a gradual disappearance of the plaque. Studies have also shown that when activated by tumor antigens, T cells differentiate into long-lasting memory T cells rather than fast-acting but short-lived effector T cells, which is more conducive to anti-tumor immunity [37]. Therefore, immune memory should play an essential role in the tumor immune cycle; however, the existing theory of the tumor immune cycle does not incorporate immune memory. We have included immune memory in the tumor immune cycle and divided it into a large cycle (grey arrows) and a small cycle with the assistance of immune memory (green arrows). The large cycle begins at antigen presentation, while the small cycle starts with memory T cells (Fig. 10).

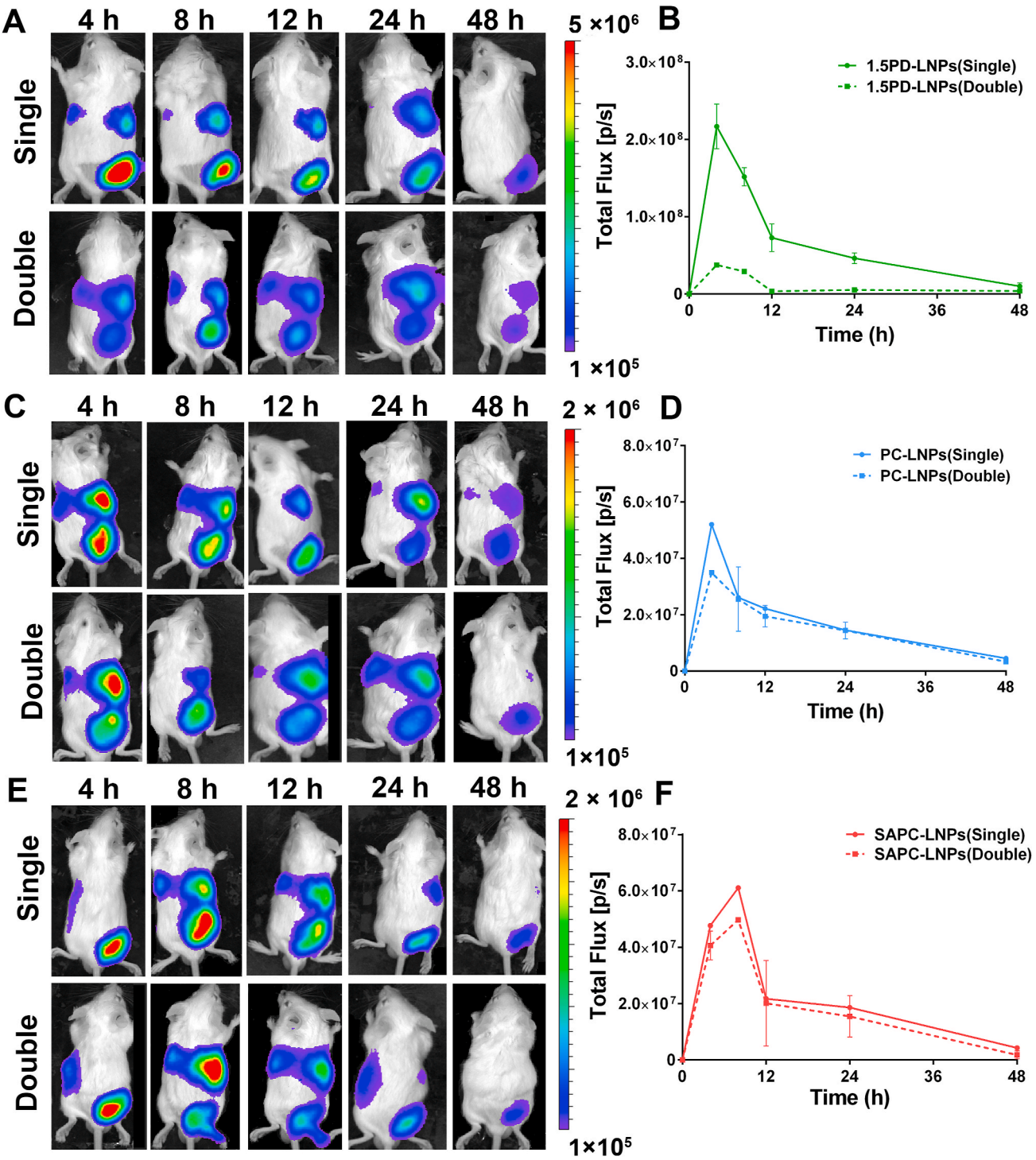

Fig. 11. Bioluminescence imaging. (A) Bioluminescence imaging, and (B) total flux-time curve of mice at 4 h, 8 h, 12 h, 24 h, and 48 h after the first and second injection of 1.5PD-LNPs. (C) Bioluminescence imaging, and (D) total flux-time curve of mice at 4 h, 8 h, 12 h, 24 h, and 48 h after the first and second injection of PC-LNPs. (E) Bioluminescence imaging, and (F) total flux-time curve of mice at 4 h, 8 h, 12 h, 24 h, and 48 h after the first and second injection of SAPC-LNPs.

3.7. Repeated administration of SAPC-LNPs generate weak immune memory to LNPs

Immune memory is the foundation of the protective immunity provided by vaccines [38]. However, not all immune memories are favorable for vaccine effectiveness. However, not all immune memories are beneficial for vaccine effectiveness. The immune memory of LNPs can accelerate the clearance of LNPs after repeated injection, which may compromise the preventive efficacy of vaccines [39]. The mRNA-LNPs vaccine contains 1.5mol% PEG-lipids; since most PEG lipids are distributed in the outer layer of LNPs, the PEG density on the surface of LNPs is much higher than 1.5 % [40], and these PEG lipids are usually non-cleavable. Although traditionally considered non-immunogenic [41], anti-PEG antibodies have been detected that expedite blood clearance of LNPs and activate the classical complement pathway [42]. These two properties can hinder clinical translation of mRNA-LNPs delivery because multiple injections are likely to be part of the treatment regimen.

We tested whether the effect of different LNPs was weakened by repeated intramuscular injections over a short period of time. The PC-LNPs, SAPC-LNPs, and 1.5PD-LNPs encapsulated with Fluc mRNA were used for repeated intramuscular injection at a time interval of 5 days. The repeated injection of 1.5PD-LNPs induced rapid clearance of LNPs, resulting in a decrease in Fluc expression to 10 % compared to that after a single injection (Fig. 11A and. B). However, repeated injection of SAPC-LNPs or PC-LNPs only resulted in a slight decrease in protein expression levels (Fig. 11C–F), indicating that the immune memory produced by SAPC-LNPs during repeated injection is weak immune memory. The application of cleavable PEG and SA modification significantly contributed to these results. As an endogenous substance, SA has low immunogenicity. The cleavable PEG-lipid dropping from the LNPs further reduces the immunogenicity of LNPs. Some studies have shown that PEGylated nanoparticles are more immunogenic than PEG molecules.

Although PEG-lipids used in commercial LNPs vaccines have short acyl side chains, which causes about 2 % [43] of them to desorbed from LNPs per minute during intravenous injection, our study still produced a strong ABC phenomenon when 1.5PD-LNPs were repeatedly injected intramuscularly. This indicates that 1.5PD-LNPs still possess strong immune memory and the desorption rate of $mPEG_{2000}DMG$ in muscle tissue is not as fast as in the bloodstream. The rate of PEG-lipid desorption is related to the degree of dilution and hydrodynamic factors of the dilution medium. Intramuscular injection and subcutaneous injection are common routes for vaccine administration, and the dilution and shear stress experienced by LNPs through these two routes should be significantly different from intravenous administration. Therefore, it is necessary to re-evaluate the rate of uncleavable PEG-lipid desorption used in commercially available vaccines during intramuscular and subcutaneous injections to further assess the effect of different administration modes on the immune memory strength of LNPs. Additionally, we also observed a delayed peak expression level of Fluc after SAPC-LNPs injection compared with other groups. Although the reason for this delay remains unclear, it suggests that SAPC-LNPs may have higher safety levels, especially when applied to cytogenic therapies where rapid cytokine expression can trigger acute inflammation that may be life-threatening.

4. Conclusion

We prepared a vaccine consisting of sialic acid (SA) - lipid derivative and cleavable PEG - lipid derivative co-modified LNPs (SAPC-LNPs). It was found that the SAPC-LNPs vaccine provided longer duration of preventive protection compared to commercially available vaccines, with a one-year protection rate of 87.5 % versus 62.5 %. Immune memory was divided into robust and weak categories, and it was discovered that the durable protective efficacy of the SAPC-LNPs vaccine was associated with the establishment of robust immune memory for tumor antigens and weak immune memory for LNPs. The robust immune memory for antigens is attributed to DC-targeting and rapid endosomal escape, which contribute to efficient transfection in DCs. The weak immune memory for LNPs is linked to the co-application of cleavable PEG and SA, reducing the immunogenicity of the LNPs vector itself. For the first time, we utilized the ratio of T_{CM} to T_{EM} as an indicator to evaluate vaccine efficiency. A higher ratio indicates stronger antigen immune memory formation and longer protective effects provided by the vaccine. Importantly, it has been discovered that immune memory plays a crucial role in tumor immunity cycle, leading us towards a more comprehensive understanding of this mechanism.

CRediT authorship contribution statement

Xueying Tang: Writing – original draft, Methodology, Investigation. **Jiashuo Zhang:** Investigation. **Dezhi Sui:** Data curation. **Zihan Xu:** Investigation. **Qiongfen Yang:** Investigation. **Tianyu Wang:** Investigation. **Xiaoya Li:** Investigation. **Xinrong Liu:** Supervision. **Yihui Deng:** Writing – review & editing, Supervision, Funding acquisition. **Yanzhi Song:** Supervision, Methodology.

Declaration of competing interest

The authors declare that they have no known competing financial interests or personal relationships that could have appeared to influence the work reported in this paper.

Data availability

Data will be made available on request.

Acknowledgements

This study was supported by the National Natural Science Foundation of China (81973271).

Appendix A. Supplementary data

Supplementary data to this article can be found online at https://doi.org/10.1016/j.mtbio.2024.100988.

References

[1] X. Hou, T. Zaks, R. Langer, Y. Dong, Lipid nanoparticles for mRNA delivery, Nat. Rev. Mater. 6 (2021) 1078–1094.
[2] B.N. Aldosari, I.M. Alfagih, A.S. Almurshedi, Lipid nanoparticles as delivery systems for RNA-based vaccines, Pharmaceutics 13 (2021) 206.
[3] K. Paunovska, D. Loughrey, J.E. Dahlman, Drug delivery systems for RNA therapeutics, Nat. Rev. Genet. (2022) 1–16.
[4] A.E. Felber, M.-H. Dufresne, J.-C. Leroux, pH-sensitive vesicles, polymeric micelles, and nanospheres prepared with polycarboxylates, Adv. Drug Deliv. Rev. 64 (2012) 979–992.
[5] A.S. Abu Lila, H. Kiwada, T. Ishida, The accelerated blood clearance (ABC) phenomenon: clinical challenge and approaches to manage, J. Contr. Release 172 (2013) 38–47, https://doi.org/10.1016/j.jconrel.2013.07.026.
[6] Y. Granot, D. Peer, Delivering the right message: challenges and opportunities in lipid nanoparticles-mediated modified mRNA therapeutics-An innate immune system standpoint, Semin. Immunol. 34 (2017) 68–77, https://doi.org/10.1016/j.smim.2017.08.015.
[7] Y. Ju, W.S. Lee, E.H. Pilkington, H.G. Kelly, S. Li, K.J. Selva, et al., Anti-PEG antibodies boosted in humans by SARS-CoV-2 lipid nanoparticle mRNA vaccine, ACS Nano 16 (2022) 11769–11780.
[8] Y. Ju, J.M. Carreño, V. Simon, K. Dawson, F. Krammer, S.J. Kent, Impact of anti-PEG antibodies induced by SARS-CoV-2 mRNA vaccines, Nat. Rev. Immunol. 23 (2023) 135–136, https://doi.org/10.1038/s41577-022-00825-x.
[9] W.A. Chen, D.Y. Chang, B.M. Chen, Y.C. Lin, Y. Barenholz, S.R. Roffler, Antibodies against poly(ethylene glycol) activate innate immune cells and induce hypersensitivity reactions to PEGylated nanomedicines, ACS Nano 17 (2023) 5757–5772, https://doi.org/10.1021/acsnano.2c12193.
[10] B.M. Chen, T.L. Cheng, S.R. Roffler, Polyethylene glycol immunogenicity: theoretical, clinical, and practical aspects of anti-polyethylene glycol antibodies, ACS Nano 15 (2021) 14022–14048, https://doi.org/10.1021/acsnano.1c05922.
[11] G.T. Kozma, T. Mészáros, I. Vashegyi, T. Fülöp, E. Örfi, L. Dézsi, et al., Pseudo-anaphylaxis to polyethylene glycol (PEG)-Coated liposomes: roles of anti-PEG IgM and complement activation in a porcine model of human infusion reactions, ACS Nano 13 (2019) 9315–9324, https://doi.org/10.1021/acsnano.9b03942.
[12] S. Sabnis, E.S. Kumarasinghe, T. Salerno, C. Mihai, T. Ketova, J.J. Senn, et al., A novel amino lipid series for mRNA delivery: improved endosomal escape and sustained pharmacology and safety in non-human primates, Mol. Ther. 26 (2018) 1509–1519, https://doi.org/10.1016/j.ymthe.2018.03.010.
[13] Q. Cheng, T. Wei, L. Farbiak, L.T. Johnson, S.A. Dilliard, D.J. Siegwart, Selective organ targeting (SORT) nanoparticles for tissue-specific mRNA delivery and CRISPR–Cas gene editing, Nat. Nanotechnol. 15 (2020) 313–320.
[14] X. Wang, S. Liu, Y. Sun, X. Yu, S.M. Lee, Q. Cheng, et al., Preparation of selective organ-targeting (SORT) lipid nanoparticles (LNPs) using multiple technical methods for tissue-specific mRNA delivery, Nat. Protoc. 18 (2023) 265–291, https://doi.org/10.1038/s41596-022-00755-x.
[15] A. Sette, S. Crotty, Immunological memory to SARS-CoV-2 infection and COVID-19 vaccines, Immunol. Rev. 310 (2022) 27–46, https://doi.org/10.1111/imr.13089.
[16] M. Kim, M. Jeong, S. Hur, Y. Cho, J. Park, H. Jung, et al., Engineered ionizable lipid nanoparticles for targeted delivery of RNA therapeutics into different types of cells in the liver, Sci. Adv. 7 (2021), https://doi.org/10.1126/sciadv.abf4398.
[17] E. Kon, N. Ad-El, I. Hazan-Halevy, L. Stotsky-Oterin, D. Peer, Targeting cancer with mRNA-lipid nanoparticles: key considerations and future prospects, Nat. Rev. Clin. Oncol. (2023), https://doi.org/10.1038/s41571-023-00811-9.

[18] X. Hou, T. Zaks, R. Langer, Y. Dong, Lipid nanoparticles for mRNA delivery, Nat. Rev. Mater. 6 (2021) 1078–1094, https://doi.org/10.1038/s41578-021-00358-0.
[19] M. Liu, Y. Su, M. Chen, J. Wang, M. Liu, Y. Dai, et al., A preliminary study of the innate immune memory of Kupffer cells induced by PEGylated nanoemulsions, J. Contr. Release 343 (2022) 657–671, https://doi.org/10.1016/j.jconrel.2021.12.025.
[20] C.B. Roces, G. Lou, N. Jain, S. Abraham, A. Thomas, G.W. Halbert, et al., Manufacturing considerations for the development of lipid nanoparticles using microfluidics, Pharmaceutics 12 (2020) 1095.
[21] M. Yanez Arteta, T. Kjellman, S. Bartesaghi, S. Wallin, X. Wu, A.J. Kvist, et al., Successful reprogramming of cellular protein production through mRNA delivered by functionalized lipid nanoparticles, Proc. Natl. Acad. Sci. USA 115 (2018) E3351–E3360.
[22] S. Rauch, J. Lutz, A. Kowalczyk, T. Schlake, R. Heidenreich, RNActive® Technology: Generation and Testing of Stable and Immunogenic mRNA Vaccines, RNA Vaccines: Methods and Protocols, 2017, pp. 89–107.
[23] C.A. Alabi, K.T. Love, G. Sahay, H. Yin, K.M. Luly, R. Langer, et al., Multiparametric approach for the evaluation of lipid nanoparticles for siRNA delivery, Proc. Natl. Acad. Sci. U. S. A. 110 (2013) 12881–12886, https://doi.org/10.1073/pnas.1306529110.
[24] E. Gutiérrez-Martínez, S. Benet Garrabé, N. Mateos, I. Erkizia, J.A. Nieto-Garai, M. Lorizate, et al., Actin-regulated Siglec-1 nanoclustering influences HIV-1 capture and virus-containing compartment formation in dendritic cells, Elife (2023) 12, https://doi.org/10.7554/eLife.78836.
[25] S. Prenzler, S. Rudrawar, M. Waespy, S. Kelm, S. Anoopkumar-Dukie, T. Haselhorst, The role of sialic acid-binding immunoglobulin-like-lectin-1 (siglec-1) in immunology and infectious disease, Int. Rev. Immunol. 42 (2023) 113–138, https://doi.org/10.1080/08830185.2021.1931171.
[26] M. Klaas, S. Dubock, D.J.P. Ferguson, P.R. Crocker, Sialoadhesin (CD169/Siglec-1) is an extended molecule that escapes inhibitory cis-interactions and synergizes with other macrophage receptors to promote phagocytosis, Glycoconj. J. 40 (2023) 213–223, https://doi.org/10.1007/s10719-022-10097-1.
[27] Z. Chen, Y. Tian, J. Yang, F. Wu, S. Liu, W. Cao, et al., Modular design of biodegradable ionizable lipids for improved mRNA delivery and precise cancer metastasis delineation in vivo, J. Am. Chem. Soc. 145 (2023) 24302–24314, https://doi.org/10.1021/jacs.3c09143.
[28] A.M. Dudek, S. Martin, A.D. Garg, P. Agostinis, Immature, semi-mature, and fully mature dendritic cells: toward a DC-cancer cells interface that augments anticancer immunity, Front. Immunol. 4 (2013) 438.
[29] M.B. Lutz, G. Schuler, Immature, semi-mature and fully mature dendritic cells: which signals induce tolerance or immunity? Trends Immunol. 23 (2002) 445–449.
[30] N.P. Klein, N. Lewis, K. Goddard, B. Fireman, O. Zerbo, K.E. Hanson, et al., Surveillance for adverse events after COVID-19 mRNA vaccination, JAMA 326 (2021) 1390–1399.
[31] J.H. Im, E. Kim, E. Lee, Y. Seo, Y. Lee, Y. Jang, et al., Adverse events with the Pfizer-BioNTech COVID-19 vaccine among Korean healthcare workers, Yonsei Med. J. 62 (2021) 1162.
[32] B.Z. Igyártó, S. Jacobsen, S. Ndeupen, Future considerations for the mRNA-lipid nanoparticle vaccine platform, Current Opinion in Virology 48 (2021) 65–72.
[33] B. Cabanillas, N. Novak, C.A. Akdis, The form of PEG matters: PEG conjugated with lipids and not PEG alone could be the specific form involved in allergic reactions to COVID-19 vaccines, Allergy 77 (2022) 1658–1660, https://doi.org/10.1111/all.15187.
[34] N. Iwamura, K. Eguchi, T. Koga, K. Tsutsumi, T. Araki, T. Aramaki, et al., Hypocomplementemic urticarial vasculitis case with hemophagocytic lymphohistiocytosis following SARS-CoV-2 mRNA vaccination, Immunol Med 46 (2023) 97–107, https://doi.org/10.1080/25785826.2023.2193286.
[35] G.T. Kozma, T. Shimizu, T. Ishida, J. Szebeni, Anti-PEG antibodies: properties, formation, testing and role in adverse immune reactions to PEGylated nano-biopharmaceuticals, Adv. Drug Deliv. Rev. 154–155 (2020) 163–175, https://doi.org/10.1016/j.addr.2020.07.024.
[36] M.C. Castells, E.J. Phillips, Maintaining safety with SARS-CoV-2 vaccines, N. Engl. J. Med. 384 (2021) 643–649, https://doi.org/10.1056/NEJMra2035343.
[37] A. Guo, H. Huang, Z. Zhu, M.J. Chen, H. Shi, S. Yuan, et al., cBAF complex components and MYC cooperate early in CD8(+) T cell fate, Nature 607 (2022) 135–141, https://doi.org/10.1038/s41586-022-04849-0.
[38] A. Ziogas, M.G. Netea, Trained immunity-related vaccines: innate immune memory and heterologous protection against infections, Trends Mol. Med. 28 (2022) 497–512, https://doi.org/10.1016/j.molmed.2022.03.009.
[39] G. Besin, J. Milton, S. Sabnis, R. Howell, C. Mihai, K. Burke, et al., Accelerated blood clearance of lipid nanoparticles entails a biphasic humoral response of B-1 followed by B-2 lymphocytes to distinct antigenic moieties, Immunohorizons 3 (2019) 282–293, https://doi.org/10.4049/immunohorizons.1900029.
[40] Y. Bavli, B.M. Chen, G. Gross, A. Hershko, K. Turjeman, S. Roffler, et al., Anti-PEG antibodies before and after a first dose of Comirnaty® (mRNA-LNP-based SARS-CoV-2 vaccine), J. Contr. Release 354 (2023) 316–322, https://doi.org/10.1016/j.jconrel.2022.12.039.
[41] J. Zhao, Q. Yuan, H. Wang, W. Liu, X. Liao, Y. Su, et al., Antibody responses to SARS-CoV-2 in patients with novel coronavirus disease 2019, Clin. Infect. Dis. 71 (2020) 2027–2034, https://doi.org/10.1093/cid/ciaa344.
[42] A. Ruggiero, C. Piubelli, L. Calciano, S. Accordini, M.T. Valenti, L.D. Carbonare, et al., SARS-CoV-2 vaccination elicits unconventional IgM specific responses in naïve and previously COVID-19-infected individuals, EBioMedicine 77 (2022) 103888, https://doi.org/10.1016/j.ebiom.2022.103888.
[43] B.L. Mui, Y.K. Tam, M. Jayaraman, S.M. Ansell, X. Du, Y.Y. Tam, et al., Influence of polyethylene glycol lipid desorption rates on pharmacokinetics and pharmacodynamics of siRNA lipid nanoparticles, Mol. Ther. Nucleic Acids 2 (2013) e139, https://doi.org/10.1038/mtna.2013.66.